Radiologic-Pathologic Correlation of Primary Retroperitoneal Neoplasms

Khalid Al-Dasuqi, MD
Lina Irshaid, MD
Mahan Mathur, MD

Abbreviations: ASPS = alveolar soft-part sarcoma, FDG = fluorodeoxyglucose, MPNST = malignant peripheral nerve sheath tumor, RMS = rhabdomyosarcoma, WHO = World Health Organization

RadioGraphics 2020; 40:1631–1657

https://doi.org/10.1148/rg.2020200015

Content Codes: CT GU MR

From the Department of Radiology and Biomedical Imaging (K.A.D., M.M.) and Department of Pathology (L.I.), Yale School of Medicine, 333 Cedar St, PO Box 208042, Room TE-2, New Haven, CT 06520. Recipient of a Certificate of Merit award for an education exhibit at the 2019 RSNA Annual Meeting. Received February 14, 2020; revision requested March 19 and received April 16; accepted April 17. For this journal-based SA-CME activity, the authors, editor, and reviewers have disclosed no relevant relationships. **Address correspondence to** M.M. (e-mail: *mahan.mathur@yale.edu*).

SA-CME LEARNING OBJECTIVES

After completing this journal-based SA-CME activity, participants will be able to:

- Describe the fascial planes and spaces of the retroperitoneal compartments.
- Characterize solid and cystic retroperitoneal neoplasms based on their imaging features.
- Correlate imaging features with gross and microscopic histologic findings.

See rsna.org/learning-center-rg.

Primary neoplasms that originate in the soft tissue of the retroperitoneum are rare, but they are often malignant and can grow to a substantial size at clinical presentation. Although imaging findings can be nonspecific, knowledge of some distinguishing imaging features and clinical and epidemiologic considerations can aid the radiologist in narrowing the differential diagnosis or, in some cases, providing a specific diagnosis. Some of the more important findings at cross-sectional imaging that can facilitate this assessment include tumor size and location (eg, presacral, paravertebral, or in the organ of Zuckerkandl); tissue composition (eg, fat, fibrous tissue, cystic components, or myxoid matrix), including assessment of the signal intensity of the lesion at T2-weighted MRI; degree of vascularization; and relationship to adjacent structures (ie, invasion of vascular structures such as the inferior vena cava). This assessment is further enhanced by an understanding of the gross and microscopic histologic appearances of these neoplasms. Primary solid retroperitoneal neoplasms are grouped and presented according to their primary soft-tissue element (eg, adipocytic, smooth muscle, fibroblastic, neurogenic, or skeletal muscle). Brief discussions of primary cystic retroperitoneal neoplasms and some miscellaneous neoplasms that do not fit into the aforementioned categories follow. An imaging algorithm to ensure a systematic approach to diagnosis of these lesions is also provided, which will allow the radiologist to provide more accurate interpretations for their referring providers, thus ensuring optimal patient treatment.

Online DICOM image stacks and supplemental material are available for this article.

Introduction

Primary malignant tumors that originate in the soft tissue of the retroperitoneum (ie, outside the solid retroperitoneal organs such as the kidneys, adrenal glands, and portions of the small and large bowel) are rare. In one review (1) of 25 647 malignant neoplasms from a tumor registry, retroperitoneal tumors accounted for 0.16% of all tumors. Nevertheless, 79%–90% of all retroperitoneal tumors are malignant, and they are associated with relatively high mortality rates, owing partly to the nonspecific symptoms, or lack thereof, in patients at presentation (2). However, these numbers are derived from observational studies that date back to 1950, when all cases of retroperitoneal lymphoma were historically considered to arise from the retroperitoneal soft tissue. Today, our understanding of the origin of retroperitoneal lymphoma is more nuanced, so the actual prevalence of primary malignant retroperitoneal tumors may be lower than previously reported.

An earlier incorrect version of this article appeared in print. The online version is correct.

TEACHING POINTS

- The presence of incomplete fat suppression at MRI, thick or irregular capsules or septa, internal nodular enhancement, or necrosis in a retroperitoneal fat-containing mass should raise suspicion for a lipomatous sarcoma, and biopsy and/or surgical resection are warranted in those cases.
- Myxoid liposarcomas are often predominantly nonfatty, with a cystic appearance at CT and MRI due to the extracellular myxoid matrix (hypoattenuating compared with muscle at CT, high signal intensity at T2-weighted MRI, and low signal intensity at T1-weighted MRI). However, unlike cystic lesions, myxoid liposarcomas demonstrate varying amounts of contrast material enhancement. While they generally contain a paucity of fat, the presence of a small amount of fat in lacy septa or nodular components is pathognomonic for myxoid liposarcomas.
- A large non–fat-containing retroperitoneal mass with involvement of a contiguous vessel and varying internal necrosis should raise the possibility of a leiomyosarcoma.
- At T2-weighted MRI, diffuse high signal intensity (a "lightbulb" appearance) has often been described in paragangliomas. However, a more complex appearance is frequently observed because of the signal heterogeneity that is associated with hemorrhage and/or necrosis.
- At CT, lymphatic malformations often appear as a uniformly cystic mass and exhibit attenuation that is near that of water. The walls and/or septa are rarely perceptible, and septal enhancement is difficult to appreciate at CT. They classically can involve more than one retroperitoneal compartment and can appear as an elongated and insinuating mass, which is an important imaging clue.

CT and MRI are the primary imaging modalities for the diagnosis and follow-up of retroperitoneal lesions. Determining the anatomic extent and key imaging features of primary retroperitoneal neoplasms is crucial for providing an accurate diagnosis and is important in selecting the appropriate patient treatment. This can be facilitated by an understanding of the gross and microscopic histologic features of the different lesions. Histologic subtyping also is important in prognostication and determination of the appropriate treatment regimen in patients with primary retroperitoneal neoplasms.

After we review the abdominal retroperitoneal anatomy and discuss how to recognize the retroperitoneal origin of a mass, we elaborate on several types of common and uncommon primary retroperitoneal neoplasms, highlighting key epidemiologic, clinical, imaging, and histologic features that allow the radiologist to provide an accurate diagnosis. A summary of these features can be found in the Table. An algorithmic approach to evaluating these lesions at MRI is presented online. (Fig E1).

Abdominal Retroperitoneal Anatomy

The retroperitoneum is divided into three compartments, the borders of which are delineated by different fascia. The most anterior compartment, known as the anterior pararenal space, is bounded anteriorly by the posterior layer of the parietal peritoneum, posteriorly by the anterior renal fascia (also known as the Gerota fascia), and laterally by the lateroconal fascia. The most posterior compartment, known as the posterior pararenal space, is bounded anteriorly by the posterior renal fascia (also known as the Zuckerkandl fascia) and posteriorly by the transversalis fascia. Medially, this space is limited by the fusion of the posterior renal and transversalis fascia with the muscular fascia, while anterolaterally, this is contiguous with the properitoneal fat. The perirenal space is bounded anteriorly by the anterior renal fascia and posteriorly by the posterior renal fascia (Fig 1a) (3).

In addition to delineating the retroperitoneal compartments, the aforementioned fascial layers have been shown to represent potentially expansile planes that allow communication of neoplastic and nonneoplastic processes between these compartments (4). The retromesenteric plane corresponds to the anterior renal fascia, the retrorenal plane corresponds to the posterior renal fascia, and the lateroconal plane corresponds to the lateroconal fascia (Fig 1a) (5). Inferiorly, these form the combined interfascial plane, which courses anteriorly to the psoas muscle, allowing communication to the pelvis (Fig 1b) (5). Some authors (6) have proposed an additional interfascial plane, termed the subfascial plane, which is located between the posterior pararenal space and the transversalis fascia. Perinephric bridging septa serve as potential channels that allow disease processes to communicate from the perirenal space to the interfascial planes (Fig 1c) (7).

Localization of Retroperitoneal Tumors

Before examining specific imaging features of the primary retroperitoneal neoplasm, the radiologist must ensure that the mass arises in the retroperitoneal soft tissues as opposed to the peritoneum or an organ that resides in the retroperitoneum. This is critically important because a mass containing macroscopic fat arising in the peritoneal cavity seldom is a liposarcoma, while a fat-containing mass arising from a retroperitoneal organ (such as the kidneys) often is a benign finding.

First, the radiologist can start by assessing how normal structures are displaced by the identified mass (8). This is especially useful because most retroperitoneal tumors are large at patient presentation, and displacement of adjacent structures is common. Masses displacing the retroperitoneal organs anteriorly (eg, the kidneys, ascending colon, descending colon, and pancreas) are

Key Imaging, Epidemiologic, Clinical, and Histologic Features of Primary Retroperitoneal Neoplasms

Category of Tumor	Key Radiologic Features	Key Epidemiologic, Clinical, and Histologic Features
Adipocytic		
Lipoma	Fat-containing mass with no/trace internal complexity	Rare in the retroperitoneum Even with no internal complexity, the mass should be considered a well-differentiated liposarcoma
Well-differentiated liposarcoma	Predominantly fat containing, with thick septa and soft-tissue nodularity (usually ≥1 cm)	Most common primary retroperitoneal sarcoma No potential to metastasize, but poor long-term survival due to high risk of local recurrence and potential for degeneration to a dedifferentiated liposarcoma
Dedifferentiated liposarcoma	Fat containing, with increasing internal complexity	Potential to metastasize Can arise in a preexisting or current well-differentiated liposarcoma
Myxoid liposarcoma	Paucity of fat, often present in septa or as small nodules Variable myxoid tissue (T2-hyperintense with variable enhancement)	Propensity to metastasize to unusual soft-tissue and bone locations
Pleomorphic liposarcoma	Trace of fat to no visible fat Heterogeneous appearance with necrosis and/or hemorrhage	Aggressive tumor May metastasize early to the lungs in 75% of patients
Smooth muscle		
Leiomyoma	Similar appearance to that of smooth muscle Hypointense at T2-weighted MRI, with variable enhancement	Uncommon Most often diagnosed in women of reproductive age, usually hormonally driven
Leiomyosarcoma	Heterogeneous mass with involvement of a contiguous vessel and variable necrosis	Second most common primary retroperitoneal sarcoma Classified as extravascular, intravascular, or a combination of both
Fibroblastic		
Solitary fibrous tumor	Heterogeneous appearance Often highly vascular with prominent collateral vessels at CT Flow voids at MRI	Most common location in the abdomen is the retroperitoneum Malignancy rate, 20%–40% Small percentage are associated with paraneoplastic syndromes, most commonly Doege-Potter syndrome (hypoglycemia due to excessive production of insulin-like growth)
Myxofibrosarcoma	Imaging appearance is dependent on histologic grade: low-grade tumors show abundant myxoid matrix, while high-grade lesions are more heterogeneous; may show "tail" sign at contrast material–enhanced T1-weighted MRI	Common extremity sarcoma in elderly patients, but retroperitoneal location is rare High rate of local recurrence regardless of grade; however, high-grade tumors are more likely to metastasize
Neurogenic		
Neurofibroma	Target sign: peripheral signal hyperintensity with central signal hypointensity	Subtypes: localized, diffuse, plexiform Neurofibromatosis 1 is associated with the presence of multiple neurofibromas or a plexiform neurofibroma

(Table continues)

more likely to be primary retroperitoneal tumors. In addition, displacement of the abdominal aorta and/or the inferior vena cava and their branches can be suggestive of a retroperitoneal mass.

Certain radiologic signs can also be used to confirm the lesion's location, including the "beak" sign, the "phantom organ" sign, the "embedded organ" sign, and the "prominent feeding artery" sign (8). The beak sign is present when the deformed edges of the organ adjacent to the index mass appear beak-shaped, suggesting that the mass originates from the organ, while

Schwannoma	Difficult to distinguish from a neurofibroma May show fascicular sign (numerous internal ringlike structures at T2-weighted MRI)	Mostly sporadic Small subset associated with neurofibromatosis Rate of successful surgical excision generally higher than that of neurofibromas Malignant degeneration rare
Malignant peripheral nerve sheath tumor	Difficult to distinguish from neurofibroma and schwannoma Clues include larger size, ill-defined borders, internal heterogeneity with necrosis and/or hemorrhage, and new or worsening neurologic deficit	Approximately 50% arise de novo The rest are seen in neurofibromatosis 1, with a small subset occurring in patients with a remote history of radiation therapy
Ganglioneuroma	Paravertebral mass Heterogeneous with a variable amount of myxoid stroma "Whorled" appearance at T2-weighted MRI	Benign tumors arise from paravertebral sympathetic ganglia Manifest most commonly in children, adolescents, and young adults Rarely secrete sufficient amounts of catecholamines to cause sympathetic symptoms (eg, flushing)
Ganglioneuroblastoma	Heterogeneous Calcifications, necrosis, and hemorrhage more common than ganglioneuroma Avid radiotracer uptake at iodine 123 (^{123}I) metaiodobenzylguanidine (MIBG) MRI in approximately 70% of cases	Malignant tumor Commonly arises in adrenal medulla Primarily affects children aged 2–4 years
Paraganglioma	Classically hyperintense at T2-weighted MRI, with hypervascularity More complex appearance is frequently observed because of hemorrhage and/or necrosis Gallium 68 (^{68}Ga) tetraazacyclododecane tetraacetic acid-octreotate (DOTATATE) PET/CT is superior for localizing and staging	Most common location in abdomen is the origin of the inferior mesenteric artery near the aortic bifurcation (organ of Zuckerkandl) Associated with multiple endocrine neoplasia syndromes and Von Hippel–Lindau syndrome
Skeletal muscle: rhabdomyosarcoma	Heterogeneous, nonspecific infiltrative appearance, with regions of necrosis	Most common soft-tissue sarcoma in children aged 15 years and younger Most commonly seen in the head or neck Retroperitoneal location seen in 7%–19% of patients
Miscellaneous		
Undifferentiated pleomorphic sarcoma	Heterogeneous nonspecific appearance; calcifications seen in 5%–20% of cases	Formerly known as malignant fibrous histiocytoma Diagnosis of exclusion
Alveolar soft-part sarcoma	Heterogeneous hypervascular mass; necrosis and hemorrhage may be present	Manifests as a painless slowly growing tumor but frequently metastasizes
Cystic		
Lymphatic malformation	Involves more than one retroperitoneal compartment Insinuates between structures Fluid-fluid levels may be seen Chylous content may be detectable with chemical-shift MRI	Considered a form of slowly growing vascular malformation Most common in the head and neck; only 5% in the abdomen Treatment is percutaneous sclerotherapy and/or surgery
Tailgut cyst/retrorectal cystic hamartoma	Uni- or multilocular cystic masses in the presacral space, with variably thick septa and occasional calcifications	Congenital lesions arising from the embryonic hindgut Treatment is surgical excision owing to risk of infection and malignant degeneration
Cystic teratoma	Presence of fat-fluid levels and calcifications (coarse or toothlike)	Germ cell neoplasms Retroperitoneal location is rare in adults

Figure 1. Normal retroperitoneal anatomy. **(a)** Axial illustration at the level of the kidneys shows the normal tricompartmental retroperitoneal spaces. The anterior pararenal space (shaded blue) is delineated anteriorly by the posterior layer of the parietal peritoneum (dashed blue line), posteriorly by the anterior renal fascia (dashed black circle), and laterally by the lateroconal fascia (dashed red circle). The posterior pararenal space (shaded green) is delineated anteriorly by the posterior renal fascia (dashed white circle) and posteriorly by the transversalis fascia (dotted green line). The perirenal space (shaded orange) is delineated anteriorly by the anterior renal fascia and posteriorly by the posterior renal fascia. The respective fascial layers can expand, giving rise to interfascial planes that allow communication across the retroperitoneal compartments. *LCP* = lateroconal plane, *RMP* = retromesenteric plane, *RRP* = retrorenal plane. **(b)** Sagittal illustration shows the retromesenteric plane (shaded blue, small solid arrow) and the retrorenal plane (shaded green, dashed arrow), which give rise to the combined interfascial plane (shaded red, thick solid arrow), which allows communication to the retroperitoneal portions of the pelvis. **(c)** Axial illustration of the right kidney shows the presence of bridging septa (white arrows) that allow communication from the perirenal space to the retromesenteric (shaded light blue) and retrorenal (shaded green) planes, respectively. Perirenal lymphatic vessels (thick solid black arrow), arteries (dashed black arrow), and veins (thin solid black arrow) are also shown. (Figures 1a and 1b adapted and reprinted, with permission, from reference 3. Figure 1c adapted and reprinted, with permission, from reference 7.)

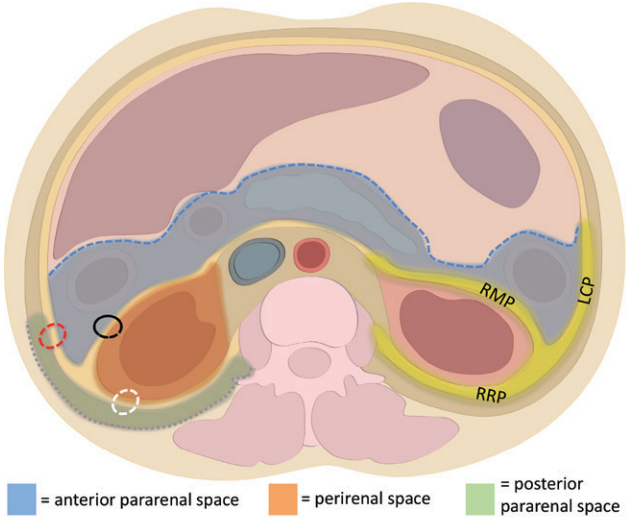

a.

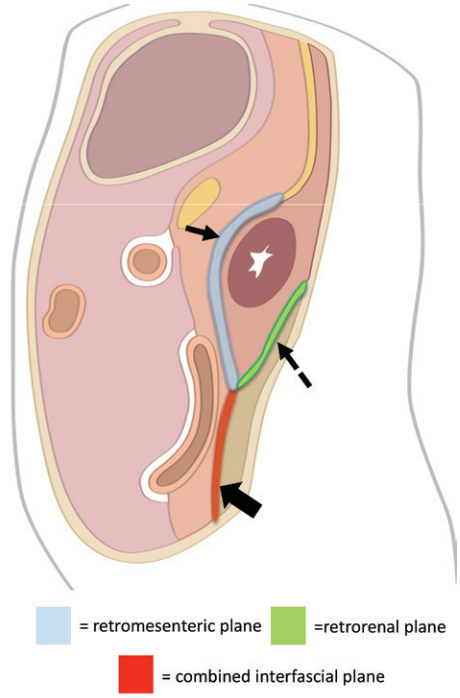

b.

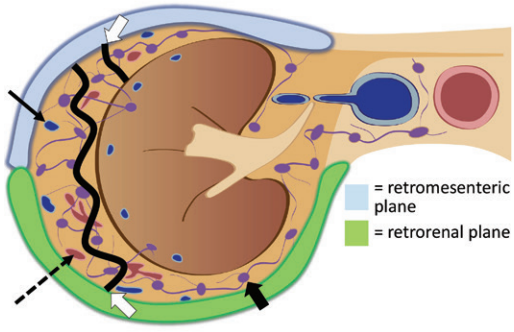

c.

the embedded organ sign is seen when the organ adjacent to the tumor is embedded in it, rather than being compressed, with a crescent shape (8). These signs are typically absent in primary retroperitoneal tumors and are more suggestive that the mass arises from an organ in the retroperitoneal cavity.

Adipocytic Tumors

Lipomas

Epidemiologic and Clinical Features.—Lipomas are benign mesenchymal tumors consisting of encapsulated mature adipose tissue (9). Lipomas are characterized on the basis of their location as *(a)* superficial lipomas, when they occur in the subcutaneous soft tissues, or *(b)* deep-seated lipomas, when they are deep to the superficial fascia. While lipomas are the most common soft-tissue tumor (accounting for 50% of all soft-tissue masses), retroperitoneal lipomas are rare, and thus, any primarily fat-containing retroperitoneal mass should be considered a well-differentiated liposarcoma rather than a lipoma, until it is proven otherwise (10).

The median age at presentation of patients with lipomas is approximately 53 years (11), according to a recent study consisting of 66 patients with a pathologically proven diagnosis of lipoma. Patients are often asymptomatic, and the lipoma only comes to clinical attention once the lesion has grown large enough to cause mass effect on adjacent organs and structures (12). Diagnosis of a retroperitoneal lipoma on the basis of biopsy alone should be made with caution because the

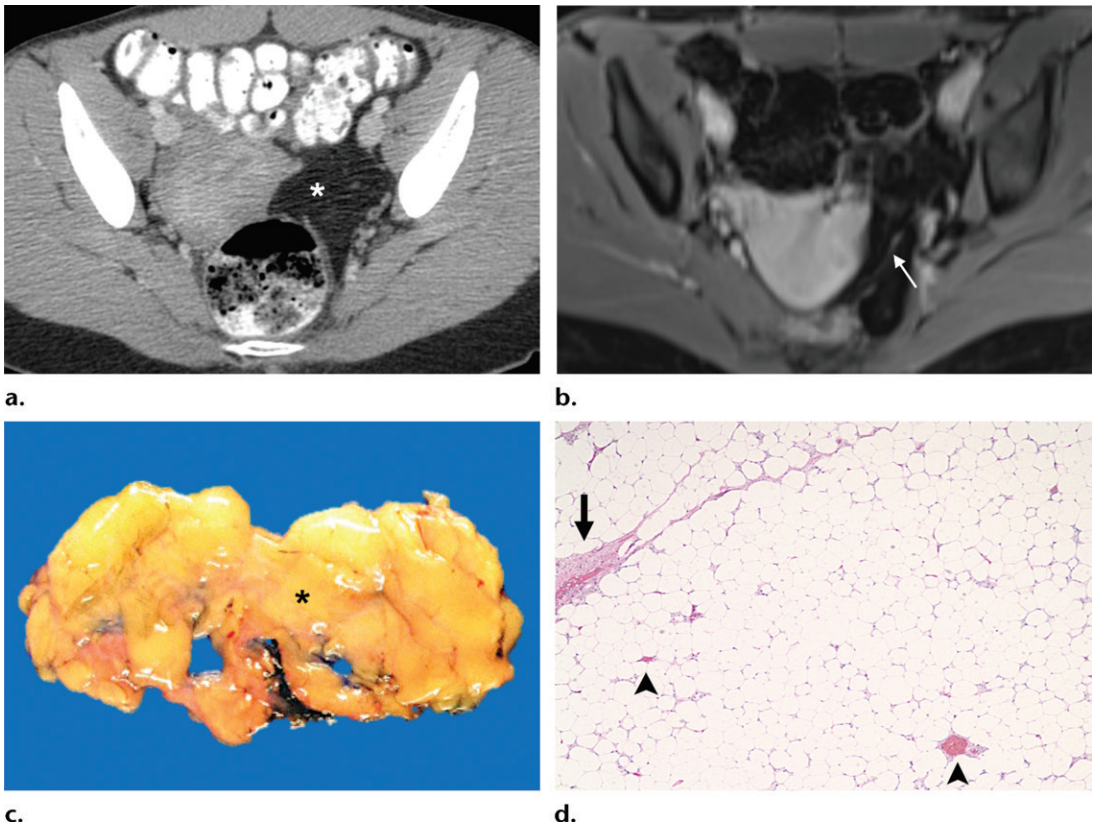

Figure 2. Lipoma in a 34-year-old woman who presented with a long-standing history of left lower quadrant pain, frequent bowel movements, and urinary urgency. **(a, b)** Axial contrast-enhanced CT image **(a)** and contrast-enhanced T1-weighted fat-saturated MR image **(b)** show a lipomatous mass (* in **a**) occupying the retroperitoneal space along the left pelvic sidewall, with a few minimally enhancing thin septa (arrow in **b**). **(c)** At gross pathologic evaluation, the mass is thinly encapsulated, soft, and yellow, with homogeneously yellow lobulated cut surfaces (*) without grossly identifiable fibrosis, necrosis, calcification, or hemorrhage. **(d)** Medium-power photomicrograph shows mature adipocytes, with minimal size variation and without nuclear atypia. (Hematoxylin-eosin stain; original magnification, ×40.) Adipocytes are divided into lobules by fibrous bands (arrow) with intermixed small- and medium-sized vessels (arrowheads).

tissue may be derived from lipoma-like areas of an otherwise under-sampled well-differentiated liposarcoma (12).

Radiologic Features.—MRI is the modality of choice for evaluation of fat-containing lesions owing to its superior soft-tissue resolution. Lipomas most often show homogeneous signal intensity at MRI that is isointense compared with subcutaneous fat during all sequences, and chemical fat saturation is key in confirming the pure lipomatous nature of the lesions. Thin septa may occasionally be present in lipomas, and they may rarely demonstrate minimal enhancement with administration of intravenous gadolinium contrast material (13).

At CT, lipomas typically appear as well-defined encapsulated masses with similar attenuation to that of subcutaneous fat (−10 to −100 HU) (Fig 2a, 2b) (14). Malignant lipomatous lesions are difficult to exclude with US alone, and follow-up MRI should be recommended. The presence of incomplete fat suppression at MRI, thick or irregular capsules or septa, internal nodular enhancement, or necrosis in a retroperitoneal fat-containing mass should raise suspicion for a lipomatous sarcoma, and biopsy and/or surgical resection are warranted in those cases (13).

Pathologic and Molecular Features.—At gross pathologic evaluation, lipomas are well-circumscribed and encapsulated tumors that display homogeneous lobulated cut surfaces, often without fibrosis, necrosis, calcification, or hemorrhage (Fig 2c). Microscopic features include mature adipocytes, with minimal size variation and without nuclear atypia. Adipocytes are divided into lobules by fibrous bands with intermixed small- and medium-sized vessels (Fig 2d).

Liposarcoma

Epidemiologic and Clinical Features.—Liposarcoma is a malignant adipose tissue tumor (9). It accounts for approximately 15% of all

soft-tissue tumors (9), with 10%–20% of liposarcomas arising in the retroperitoneum (15). Liposarcoma is the most common primary retroperitoneal sarcoma, accounting for 35% of all malignant retroperitoneal soft-tissue tumors in adult patients (16). They often manifest as large encapsulated fat-containing masses that displace adjacent structures, and average patients typically present during their fifth through seventh decades of life (15–17).

Liposarcomas are histologically divided into four subtypes including *(a)* well-differentiated liposarcoma (also called atypical lipomatous tumor when found in the extremities), *(b)* myxoid liposarcoma, *(c)* pleomorphic liposarcoma, and *(d)* dedifferentiated liposarcoma (9). Among these, well-differentiated liposarcomas are the most common, followed by the dedifferentiated subtype, with myxoid and pleomorphic liposarcomas rarely seen in the retroperitoneum (15). In one study (15) of 177 patients with retroperitoneal liposarcomas, well-differentiated tumors were found in 56% of patients, while dedifferentiated lesions were present in 37% of patients. Well-differentiated liposarcomas are considered intermediate-grade tumors, according to the World Health Organization (WHO) classification system, while the other subtypes are considered high-grade tumors (9).

Well-differentiated retroperitoneal liposarcomas have no potential to metastasize, but the long-term mortality rate can reach 22%–33% owing to a high risk of recurrence and a potential for malignant degeneration to dedifferentiated liposarcoma (17–19). The high risk of recurrence is due, in part, to the difficulty of achieving tumor-free resection margins, because tumors are often inseparable from adjacent structures (15). In one study (19) of 168 patients with retroperitoneal liposarcoma, half of the patients required resection of at least one contiguous organ. Recurrence of well-differentiated liposarcoma is associated with a higher risk of dedifferentiation (20).

Dedifferentiated liposarcomas are high-grade sarcomas that are believed to either arise de novo in a preexisting well-differentiated liposarcoma (approximately 90%) or form in a recurrent well-differentiated liposarcoma (approximately 10%) (18). Dedifferentiated liposarcomas are clinically more aggressive than well-differentiated types, with a higher propensity to recur after resection and the presence of distant metastases in approximately one-fifth of cases (20). Myxoid liposarcomas have a propensity to metastasize to unusual soft-tissue and bone locations, while pleomorphic liposarcomas can metastasize early to the lungs in up to 75% of patients (21,22).

Radiologic Features.—Liposarcomas can have a variable imaging appearance, and the amount of intratumoral fat is generally inversely proportional to the grade of the tumor. Well-differentiated liposarcomas are usually predominantly fatty at CT and MRI and may demonstrate thick septa or soft-tissue–attenuating nodularity that could exhibit mild to marked enhancement after contrast material administration (Fig 3a, 3b) (12). Other imaging features that have been shown to favor the diagnosis of well-differentiated liposarcoma over benign lipomatous tumors include a lesion size of 10 cm or larger and the presence of a soft-tissue–attenuating nodule measuring greater than or equal to 1 cm. The latter feature specifically predicted a diagnosis of well-differentiated liposarcoma over lipoma in all cases in one study (23,24). While primary retroperitoneal teratomas can also contain macroscopic fat, these are rare and may demonstrate fat-fluid levels and/or calcifications (often teethlike).

Because dedifferentiated liposarcomas are believed to arise in a preexisting well-differentiated liposarcoma, the classic imaging appearance of a dedifferentiated liposarcoma is a bimorphic mass with clear demarcation between the predominantly fatty tissue and the nonfatty solid tissue (Fig E2a; a full DICOM image stack is available online). Calcifications are seen in approximately one-fifth of cases (25). Myxoid liposarcomas are often predominantly nonfatty, with a cystic appearance at CT and MRI due to the extracellular myxoid matrix (hypoattenuating compared with muscle at CT, high signal intensity at T2-weighted MRI, and low signal intensity at T1-weighted MRI) (Fig 4a, 4b) (26). However, unlike cystic lesions, myxoid liposarcomas demonstrate varying amounts of contrast material enhancement (Fig 4c). While they generally contain a paucity of fat, the presence of a small amount of fat in lacy septa or nodular components is pathognomonic for myxoid liposarcomas. Pleomorphic liposarcomas have a variable heterogeneous imaging appearance at CT and MRI (Fig 5a–5c), often manifesting as large well-defined soft-tissue masses, with areas of necrosis and hemorrhage (12).

Pathologic and Molecular Features.—Well-differentiated liposarcomas are grossly well-circumscribed and lobulated tumors with variably firm cut surfaces (Fig 3c) (12). At microscopic evaluation, these tumors show lobules of relatively mature adipocytes of varying sizes and thickened fibrous bands containing atypical stromal cell nuclei (Fig 3d) (27). Lipoblasts may be identified but are not required for the diagnosis (28).

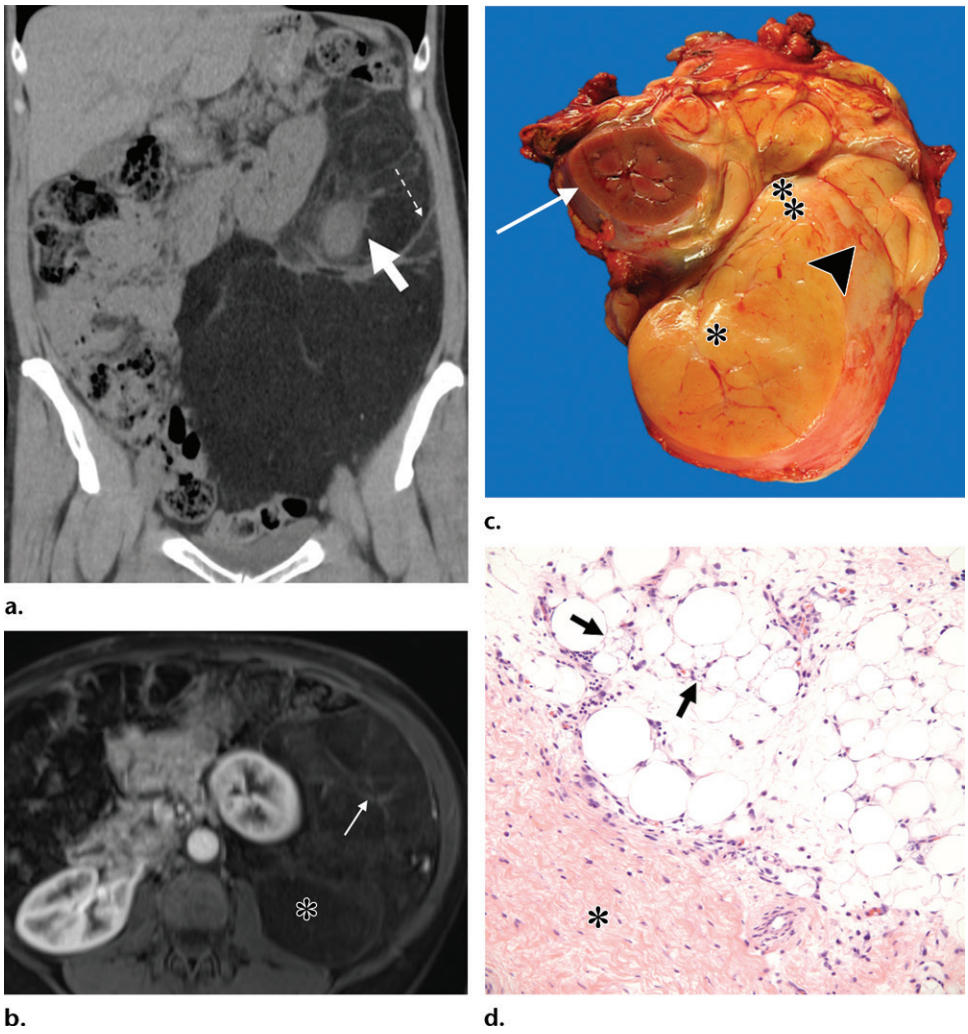

Figure 3. Well-differentiated liposarcoma in a 55-year-old woman who had increasing abdominal firmness, nausea, early satiety, and constipation. **(a)** Coronal CT image without contrast material shows a large heterogeneous well-defined predominantly fat-containing mass that displaces the left kidney medially. Internally, the mass contains a few thick septa (dashed arrow) and soft-tissue nodular components (solid arrow). **(b)** Axial contrast-enhanced fat-suppressed T1-weighted MR image shows a fat-containing mass (*) with thin enhancing septa (arrow). **(c)** Photograph of the specimen at gross pathologic examination reveals a lobulated lipomatous tumor adhering to and surrounding the kidney (arrow). The tumor displays a yellow and fatty (*) to tan-gray (**) cut surface with bands of connective tissue (arrowhead) dividing the tumor into nodules. **(d)** Medium-power photomicrograph shows lipoblasts with multiple intracytoplasmic vacuoles that indent the enlarged and hyperchromatic nucleus (arrows) and thickened fibrous bands (*), with atypical stromal cell nuclei. (Hematoxylin-eosin stain; original magnification, ×200.)

Well-differentiated liposarcomas are characterized by *MDM2* gene amplification, which can be detected by means of fluorescence in situ hybridization, polymerase chain reaction, and comparative genomic hybridization methods (29).

The gross appearance of dedifferentiated liposarcomas varies, depending on the cellular composition of the tumor. Well-differentiated liposarcoma components often appear tan-yellow, lobulated, and greasy; however, dedifferentiated components are typically variegated, with firm or fleshy cut surfaces (Fig E2b). Thorough gross sampling of all regions is critical for accurate tumor classification. Microscopically, dedifferentiated liposarcomas show a (usually abrupt) transition from a well-differentiated liposarcoma component to a high-grade sarcoma component (Fig E2c) (27,28). However, in many instances, particularly in biopsy samples, these transition areas are not identified, and morphologic overlap between dedifferentiated liposarcomas and undifferentiated pleomorphic sarcomas may complicate the distinction between the two (28). If *MDM2* amplification is detected, a diagnosis of dedifferentiated liposarcoma can be made (27,28). Moreover, poorly differentiated retroperitoneal tumors are much more likely to be dedifferentiated liposarcomas

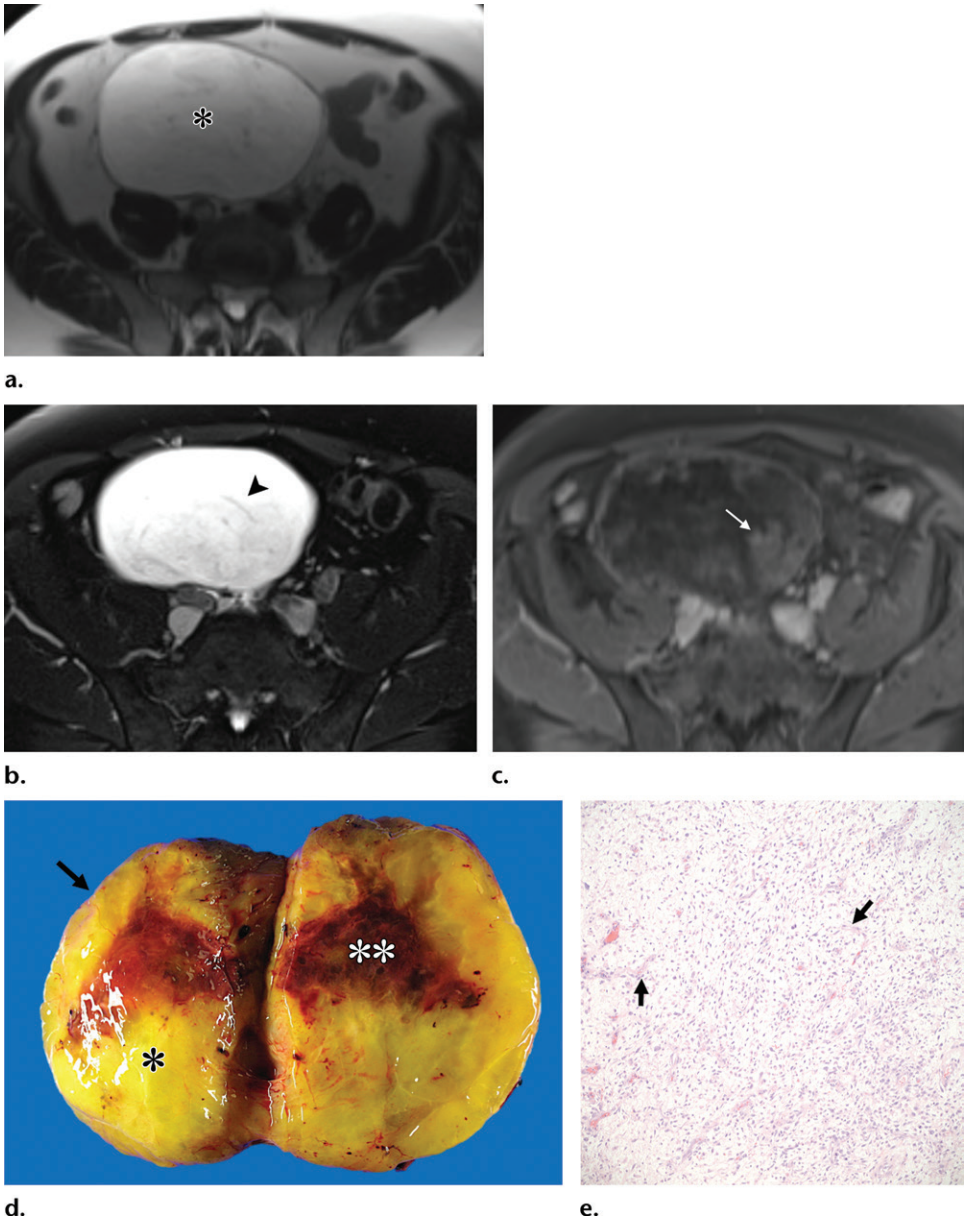

Figure 4. Myxoid liposarcoma in a 68-year-old man who presented with a 3-month history of worsening abdominal pain. **(a, b)** Axial T2-weighted MR images acquired without **(a)** and with **(b)** fat suppression reveal a hyperintense mass (* in **a**) without fat suppression. Lacelike signal hypointensity is seen (arrowhead in **b**). **(c)** Axial fat-suppressed contrast-enhanced T1-weighted MR image shows patchy areas of enhancement (arrow). **(d)** Photograph at gross pathologic examination shows a bivalved well-circumscribed mass with a tan-yellow gelatinous smooth shiny cut surface (*) and areas of hemorrhage (**) covering 30% of the total surface area. The tumor appears completely encased by a thin fibrous pseudocapsule (arrow). **(e)** Low-power photomicrograph shows abundant myxoid stroma that contains spindled tumor cells and delicate arborizing "chicken-wire" capillary vasculature (arrows). (Hematoxylin-eosin stain; original magnification, ×100.)

than they are to be undifferentiated pleomorphic sarcomas (27,28).

At gross pathologic examination, myxoid liposarcomas are well-circumscribed masses with lobulated gelatinous cut surfaces. High-grade tumors exhibit variably firm gray foci, with areas of necrosis and/or hemorrhage (Fig 4d). At microscopic evaluation , myxoid liposarcomas show an abundant myxoid stroma that contains spindled tumor cells, lipoblasts, and delicate arborizing "chicken-wire" capillary vasculature (Fig 4e) (9). More than 90% of cases harbor t(12,16)(q13;p11) translocation, involving the *DDIT3* and *FUS* genes (30).

At gross pathologic evaluation, pleomorphic liposarcomas often manifest as multinodular masses with tan-white to yellow and firm to fleshy cut surfaces (Fig 5d). Internally, areas of necrosis may be seen. Microscopic features are

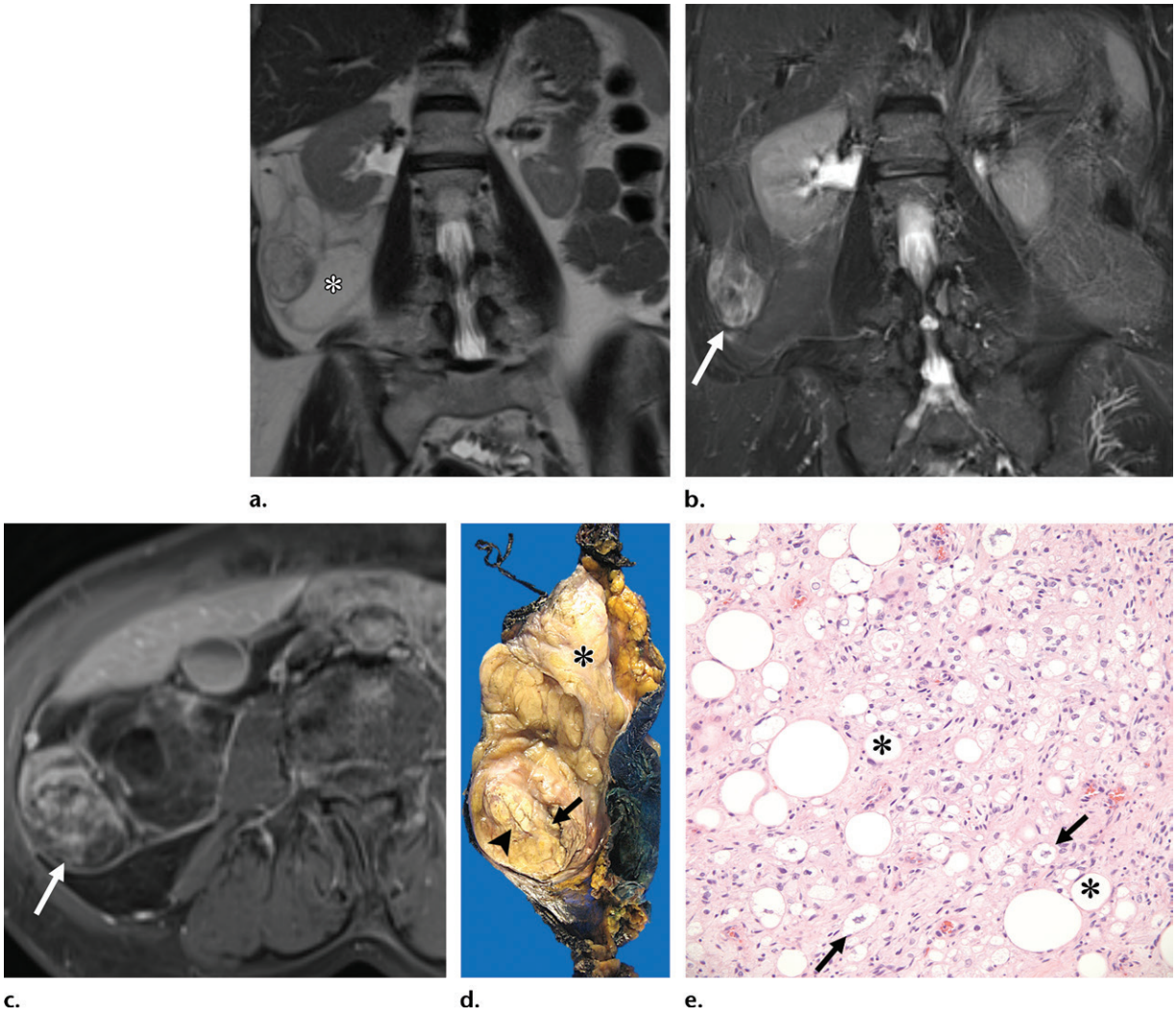

Figure 5. Pleomorphic liposarcoma in a 65-year-old woman with an 18-month history of vague abdominal pain. **(a, b)** Coronal T2-weighted MR images acquired without **(a)** and with **(b)** fat suppression reveal a fat-containing mass (* in **a**) with a hyperintense soft-tissue component (arrow in **b**). **(c)** Axial fat-suppressed contrast-enhanced T1-weighted MR image shows enhancement of the soft-tissue component (arrow). **(d)** Photograph of the mass at gross pathologic examination shows a multinodular tan-white to yellow mass that contains firm (*) to fleshy (arrowhead) cut surfaces. Occasional areas of necrosis (arrow) are identified. **(e)** Medium-power photomicrograph reveals numerous uni- (*) and multivacuolated (arrows) lipoblasts demonstrating large pleomorphic nuclei scalloped by lipid vacuoles and surrounded by pleomorphic spindle cells. (Hematoxylin-eosin stain; original magnification, ×200.)

variable but unified by the presence of univacuolated or multivacuolated lipoblasts, which must be seen to make the diagnosis (Fig 5e) (28). *Lipoblasts* are defined as cells with hyperchromatic nuclei that are scalloped by lipid vacuoles. Lipoblasts are often admixed with large high-grade pleomorphic cells (28). In a case series of 57 cases of pleomorphic liposarcomas, Hornick et al (31) noted considerable variability in the quantity of lipoblasts in the examined tumors, ranging from less than 1% to 80%. Significant variability was also noted between separate areas in the same tumor. This histologic finding may explain the intralesional variability in the imaging appearance of pleomorphic liposarcomas, as noted in Figure 5.

Smooth Muscle Tumors

Leiomyoma

Epidemiologic and Clinical Features.—Leiomyoma is a benign tumor of smooth muscle cells (9). Primary retroperitoneal leiomyomas are rare and are believed to arise from remnants of the müllerian or wolffian ducts (32). Most primary retroperitoneal leiomyomas are seen in women, but a small percentage of cases have been described in men (33,34). Up to 40% of retroperitoneal leiomyomas are associated with uterine leiomyomas (32). Pelvic retroperitoneal leiomyomas are sometimes referred to as parasitic leiomyomas when they are close to the uterus. In

patients with a parasitic leiomyoma, the tumor is believed to originate from the uterus but, over time, it becomes adherent to adjacent structures, developing an extrauterine blood supply and subsequently losing its original attachment to the uterus (32,35). Retroperitoneal leiomyomas may manifest with vague symptoms including pelvic and/or back pain and discomfort. Presenting symptoms may also be secondary to compression of adjacent structures, including urinary urgency and constipation (35).

Radiologic Features.—Retroperitoneal leiomyomas are similar in attenuation to uterine myometrial smooth muscle at CT (Fig E3a, E3b; a full DICOM image stack is available online). Calcifications are not commonly present. At T2-weighted MRI, they typically show signal hypointensity and variable enhancement with administration of contrast material (35).

Pathologic and Molecular Features.—At gross pathologic examination, leiomyomas typically manifest as well-circumscribed masses with tan whorled cut surfaces (Fig E3c). Histologic features include intersecting fascicles of uniform spindle cells, with blunt-ended nuclei and eosinophilic cytoplasms (34). Nuclear pleomorphism, mitotic activity, and necrosis are typically absent (34). In female patients, retroperitoneal leiomyomas are hormonally sensitive and frequently stain positive for estrogen and progesterone receptors (34), as shown in Figure E3d.

Leiomyosarcoma

Epidemiologic and Clinical Features.—Leiomyosarcoma is a malignant tumor of smooth muscle cells (9), with a retroperitoneal location in 12%–69% of cases (36,37). It is the second most common primary malignant retroperitoneal sarcoma, accounting for 28% of cases (26). Leiomyosarcomas are typically diagnosed during the fifth to sixth decades of life, more often in women than in men (38). Leiomyosarcoma is believed to originate from the large blood vessels in the retroperitoneum (eg, the inferior vena cava) and/or their tributaries (39). Nevertheless, leiomyosarcomas most commonly manifest as extravascular tumors (62% of cases) and are rarely completely intravascular (5%) (38). In 33% of cases, leiomyosarcomas have both an intravascular and an extravascular component (38). Similar to liposarcomas, leiomyosarcomas are often large when patients present, and symptoms are usually related to compression of adjacent structures (26,39). Metastases are seen at the time of diagnosis in 9% of patients with extravascular tumors and 23% of patients with intravascular tumors, with the lungs, liver, and peritoneum being the most common sites (39). Prognosis is typically dependent on achieving complete excision with wide negative margins (40).

Radiologic Features.—Leiomyosarcomas usually manifest as large soft-tissue masses, with internal heterogeneity and heterogeneous enhancement usually secondary to necrosis and hemorrhage (Fig 6a). The mean tumor size for lesions with and without vascular involvement has been reported as 10.4 cm and 11.3 cm, respectively (41). Calcifications are not commonly found, and adipose tissue is absent (39). Purely intravascular lesions appear as heterogeneously enhancing expansile masses. They commonly exhibit low to intermediate signal intensity at T1-weighted MRI and intermediate to high signal intensity at T2-weighted MRI. They also occasionally demonstrate fluid-fluid levels secondary to hemorrhage (26). A large non–fat-containing retroperitoneal mass with involvement of a contiguous vessel and varying internal necrosis should raise the possibility of a leiomyosarcoma (Fig 6b) (26).

Pathologic and Molecular Features.—At gross pathologic evaluation, leiomyosarcomas appear as large masses with fleshy tan-white cut surfaces. Hemorrhage and/or necrosis occur frequently (Fig 6c). Microscopically, leiomyosarcomas show intersecting fascicles of spindled cells, with abundant mitotic activity and nuclear atypia (Fig 6d, 6e) (34).

Fibroblastic Tumors

Solitary Fibrous Tumors

Epidemiologic and Clinical Features.—Solitary fibrous tumors, previously known as localized mesothelioma, are rare mesenchymal tumors that arise from fibroblast-like cells in the connective tissue (9). They are on the same spectrum of tumors as hemangiopericytomas, and the two terms are often used interchangeably (42). Approximately one-third of solitary fibrous tumors are intraabdominal, and the most common intraabdominal site is the retroperitoneum. The majority of patients are diagnosed in the fifth to seventh decades of life, but the tumor can arise at any age (42). Most solitary fibrous tumors are benign, with an estimated malignancy rate of 20%–40% (42). Retroperitoneal solitary fibrous tumors are usually initially asymptomatic and can grow large before causing symptoms. A small percentage of retroperitoneal solitary fibrous tumors are associated with paraneoplastic syndromes, most commonly Doege-Potter syndrome, which occurs in

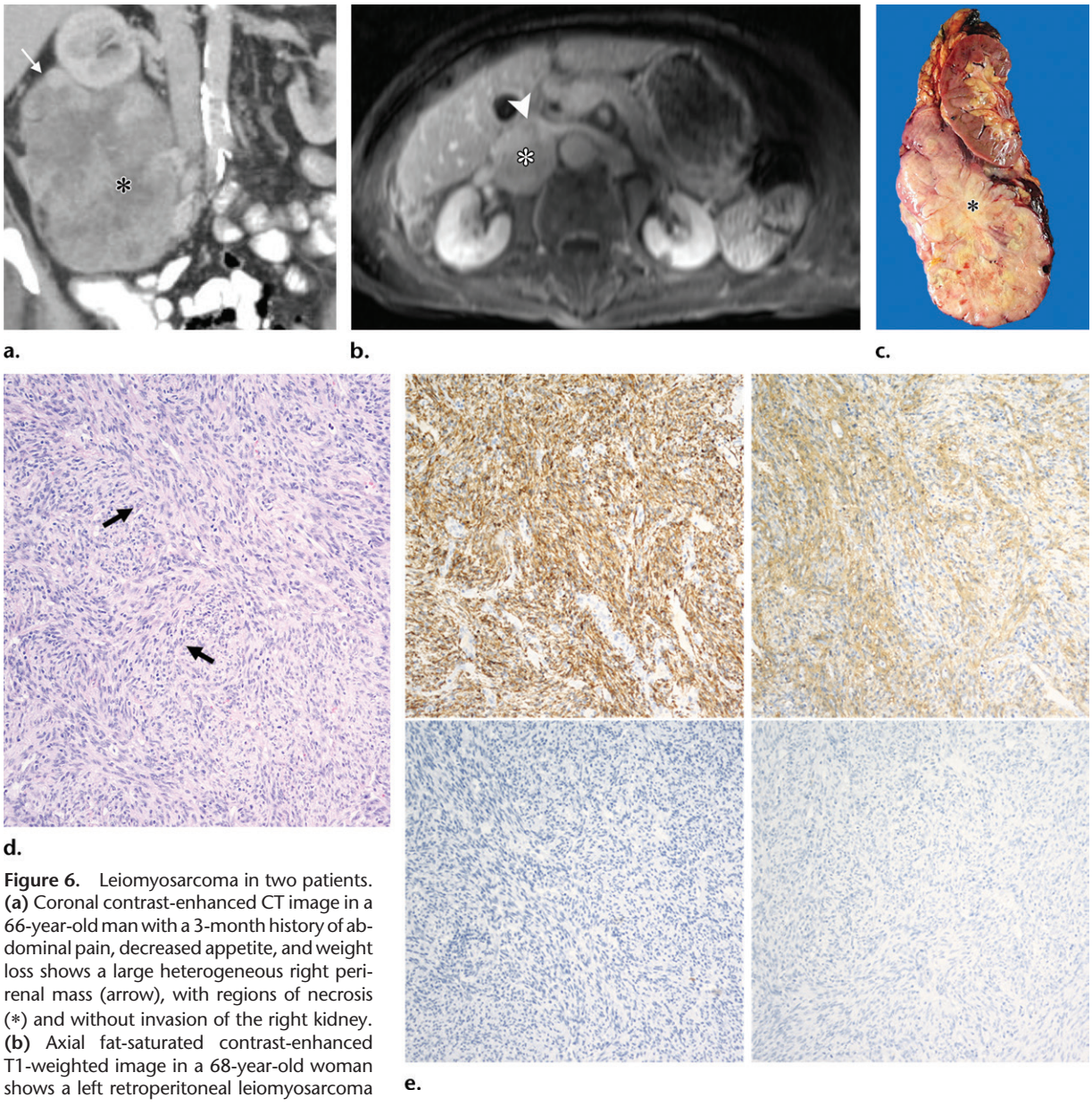

Figure 6. Leiomyosarcoma in two patients. **(a)** Coronal contrast-enhanced CT image in a 66-year-old man with a 3-month history of abdominal pain, decreased appetite, and weight loss shows a large heterogeneous right perirenal mass (arrow), with regions of necrosis (*) and without invasion of the right kidney. **(b)** Axial fat-saturated contrast-enhanced T1-weighted image in a 68-year-old woman shows a left retroperitoneal leiomyosarcoma (*) invading the inferior vena cava (arrowhead). **(c)** Photograph at gross pathologic examination of the lesion in **a** shows that the tumor is inferior to the kidney and entirely extrarenal. It displays a tan-white whorled stellate appearance (*). **(d)** Low-power photomicrograph of a specimen from the patient in **a** shows intersecting fascicles of spindled cells (arrows) with abundant mitotic activity and nuclear atypia. (Hematoxylin-eosin stain; original magnification, ×100.) **(e)** Photomicrographs of a specimen from the patient in **a** show that these cells are immunoreactive for desmin (top left) and smooth muscle actin (top right) and are negative for anaplastic lymphoma kinase (bottom left) and S100 (bottom right), supporting the diagnosis of leiomyosarcoma. (Desmin, smooth muscle actin, anaplastic lymphoma kinase, and S100 stains, respectively; original magnification, ×100.)

patients with hypoglycemia secondary to excessive production of insulin-like growth factor 2 from tumor cells (41).

Radiologic Features.—Although their imaging appearance is nonspecific, most solitary fibrous tumors show heterogeneity and are highly vascular at contrast-enhanced imaging, with prominent collateral vessels (Fig E4a) (43,44). They may rarely exhibit areas of cystic degeneration, necrosis, and calcifications (43). The signal intensity at T1-weighted and T2-weighted MRI is variable and is dependent on cellularity and the abundance of myxoid stroma and/or fibrous tissue (43). Solitary fibrous tumors are typically hypointense to isointense compared with muscle at T1-weighted MRI and hypointense at T2-weighted MRI (44). Avid contrast material enhancement is usually noted, and flow voids (manifesting as hypointense foci at T1- and T2-weighted MRI) may be present owing to prominent intralesional vessels (44).

Pathologic and Molecular Features.—Solitary fibrous tumors manifest as well-circumscribed firm masses with tan fleshy lobulated cut surfaces (Fig E4b) (45). Microscopically, these tumors are composed of round to spindled cells with a patternless arrangement around ectatic "staghorn" vessels (Fig E4c) (46). Tumor cells are characteristically positive for the *STAT6* gene, and most cases harbor 12q intrachromosomal rearrangements, resulting in *NAB2-STAT6* gene fusion (Fig E4d) (47).

Myxofibrosarcoma

Epidemiologic and Clinical Features.—Myxofibrosarcoma, previously known as a myxoid variant of malignant fibrous histiocytoma, is one of the most common malignant soft-tissue tumors in elderly patients (9,48) and shows a slight predilection for male patients (48). Low-grade lesions tend to be hypocellular and contain an abundant myxoid matrix, while high-grade lesions are hypercellular, with prominent cellular pleomorphism and atypical mitotic figures, and contain areas of hemorrhage and necrosis, with little myxoid matrix (<10% of the tumor area) (49). Despite being one of the most common sarcomas of the extremities in elderly patients, myxofibrosarcomas arising in the retroperitoneum are rare (48). Myxofibrosarcomas are associated with a relatively high rate of local recurrence after surgical resection when compared with other sarcomas, owing to the infiltrative nature of the tumor, regardless of the tumor grade. A high tumor grade correlates positively with the likelihood of metastatic spread (48).

Radiologic Features.—The imaging appearance of myxofibrosarcoma is highly dependent on the histologic tumor grade (49). Low-grade lesions are hypoattenuating compared with muscle at CT and show high T2 and low T1 signal intensity at MRI owing to the abundant myxoid matrix (49). On the other hand, high-grade lesions tend to have similar attenuation to that of muscle at CT and exhibit intermediate signal intensity at T1-weighted MRI that is secondary to hypercellularity, which is also associated with more avid contrast material enhancement (49). They can also show regions of hemorrhage and/or necrosis (Fig E5a; a full DICOM image stack is available online.). A tail-like pattern is often described (50) in myxofibrosarcoma at T2-weighted and fat-suppressed contrast-enhanced T1-weighted MRI that is secondary to the curvilinear tumoral fascial projections extending from the epicenter of the mass. In a study (50) of 96 patients with predominantly myxoid neoplasms, including myxofibrosarcoma, the presence of this "tail sign" at fat-suppressed contrast-enhanced T1-weighted MRI was 79%–90% specific for myxofibrosarcoma. This infiltrative appearance has also been shown to be associated with a higher rate of recurrence after surgical resection (50).

Pathologic and Molecular Features.—At gross pathologic examination, myxofibrosarcomas are typically multinodular growths with tan-white gelatinous cut surfaces. Areas of necrosis are commonly seen in high-grade tumors (Fig E5b). At microscopic evaluation, myxofibrosarcomas characteristically show a multinodular growth pattern, with incomplete fibrous septa, myxoid stroma–containing pleomorphic tumor cells, frequent atypical mitotic figures, and surrounding curvilinear thin-walled blood vessels (Fig E5c). The tumor grade, reflected by the degree of cellularity and atypia, is predictive of the prognosis and risk of metastasis (28).

Neurogenic Tumors

Neurofibromas

Epidemiologic and Clinical Features.—Neurofibromas are benign nerve sheath tumors that are composed of benign neoplastic Schwann cells intermixed with fibroblasts, collagen, and a myxoid matrix (51). They are often unencapsulated and interspersed with nerve fibers (51). Neurofibromas can occur in the cutaneous or deep soft tissues, and they account for 1% of all retroperitoneal tumors (52). The main subtypes are *(a)* localized, *(b)* diffuse, and *(c)* plexiform (51). Solitary localized neurofibromas are often sporadic and are not associated with neurofibromatosis type 1, whereas multiple neurofibromas or plexiform neurofibromas are nearly always associated with neurofibromatosis type 1 (51).

The age of onset in patients with solitary neurofibromas is 20–30 years, but neurofibromas in patients with neurofibromatosis type 1 often present at an earlier age (53). Malignant degeneration of neurofibromas is more common with plexiform neurofibromas or in patients with neurofibromatosis type 1 (54). Neurofibromas are frequently discovered incidentally when they arise in the retroperitoneum because they are more likely to be asymptomatic (53). Solitary localized neurofibromas are usually managed conservatively, with observation, unless they are associated with pain or a neurologic deficit, or if there is clinical concern for malignant potential. The goal of surgery is to attempt resection with preservation of nerve function (53).

Radiologic Features.—Localized neurofibromas typically manifest as well-defined minimally

Figure 7. Neurofibroma in a 54-year-old woman with an incidentally discovered left retroperitoneal mass. **(a)** Axial contrast-enhanced CT image shows a well-defined low-attenuation retroperitoneal mass (arrow) with the claw sign, which is seen in association with the displaced left psoas muscle. **(b, c)** Axial fat-saturated T2-weighted MR image **(b)** shows a homogeneously hyperintense mass (arrow), and axial fat-saturated contrast-enhanced T1-weighted MR image **(c)** shows diffuse enhancement (arrowhead in **c**). **(d)** Axial T2-weighted MR image with fat suppression in an 18-year-old woman with neurofibroma shows the classic target sign, as evidenced by the characteristic central area of low signal intensity surrounded by a rim of high signal intensity (arrowhead). **(e)** Photograph of gross pathologic specimen shows that the mass seen in **a–c** is well circumscribed with a solid pale yellow and homogeneous cut surface. **(f)** High-power photomicrograph shows a moderately cellular proliferation of loosely arranged ovoid to spindle cells with small wavy nuclei (arrows) in a myxedematous stromal matrix. (Hematoxylin-eosin stain; original magnification, ×400.) The lesional cells have benign cytologic features and lack substantial mitotic activity.

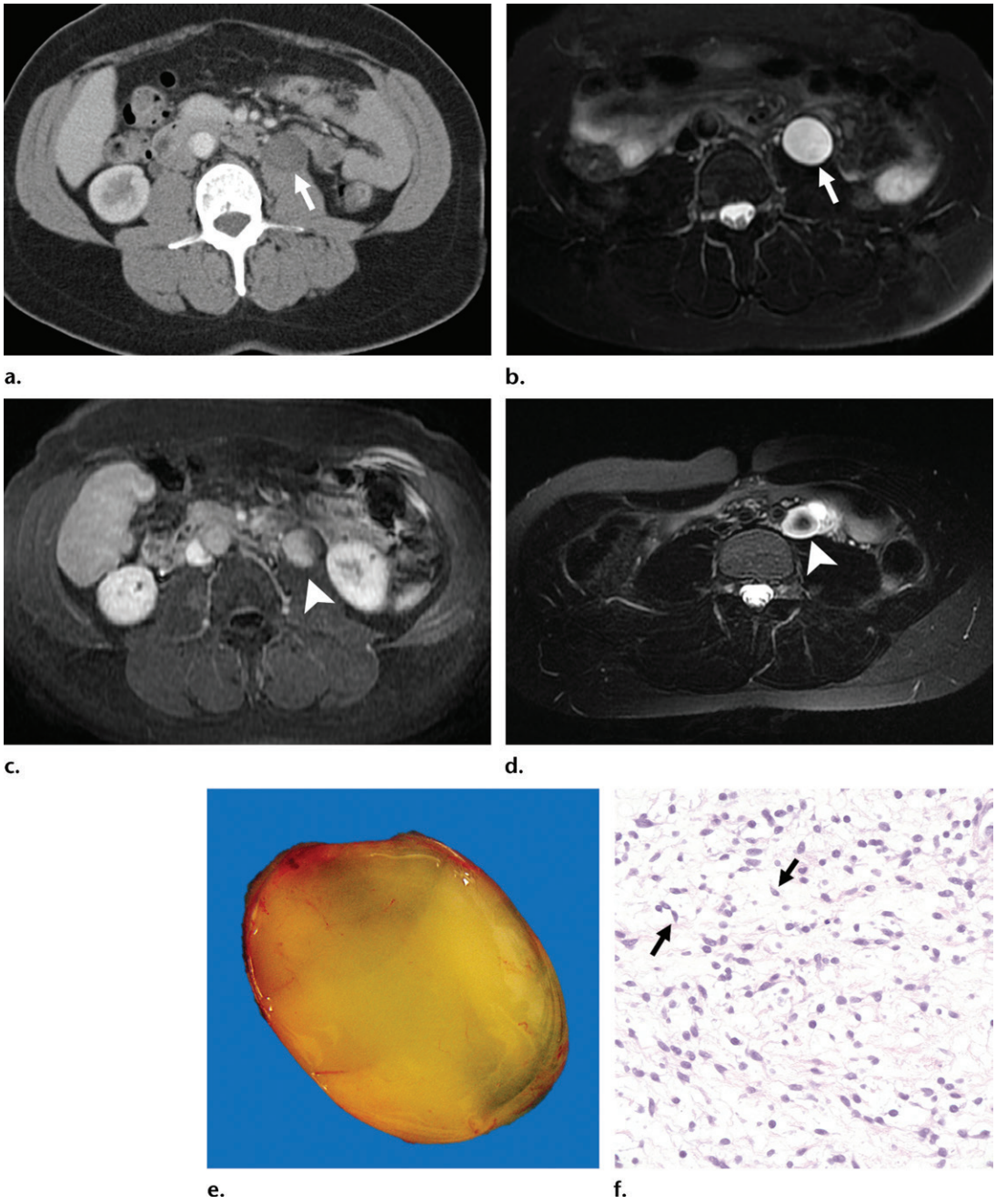

enhancing hypoattenuating masses (20–40 HU) at CT (Fig 7a) (53). They often show signal isointensity to hypointensity compared with muscle at T1-weighted MRI and signal hyperintensity at fluid-sensitive MRI, with variable enhancement (Fig 7b, 7c) (53). Neurofibromas can variably demonstrate a target sign, which consists of a central focus of low signal intensity that is presumed to reflect the centrally dense fibrocollagenous tissue, surrounded by peripheral hyperintensity, which is thought to be secondary to the peripheral myxoid matrix at T2-weighted

MRI (Fig 7d) (55). Plexiform neurofibromas tend to manifest as large infiltrative multilobulated masses or a conglomerate of masses along the nerve fibers (56). Retroperitoneal plexiform neurofibromas tend to be bilateral, symmetric, and parallel to the psoas muscle, which can be an important imaging clue to differentiate them from other retroperitoneal sarcomas (56).

Pathologic and Molecular Features.—At gross pathologic evaluation, most neurofibromas manifest as well-circumscribed unencapsulated masses with pale-yellow homogeneous cut surfaces (Fig 7e). Plexiform neurofibromas tend to be larger, multinodular, and elongated (51). Microscopically, neurofibromas exhibit hypocellular to moderately cellular proliferations of spindle cells with small wavy nuclei in a myxoedematous stromal matrix (Fig 7f) (51). Tumor cells are cytologically benign and lack substantial mitotic activity. Scattered mast cells are commonly seen (51).

Schwannomas

Epidemiologic and Clinical Features.—Schwannomas, also known as neurolemmas, are another type of benign nerve sheath tumor that account for 4% of all retroperitoneal tumors (56). As opposed to neurofibromas, they are exclusively made of benign neoplastic Schwann cells and are separable from the nerve fibers (51). Thus, they tend to grow eccentrically from peripheral nerve fibers (51). Schwannomas can occur at any age but are more common between the second and fifth decades of life (51). Most cases are sporadic, with the exception of a small fraction of cases that can be associated with neurofibromatosis type 2 (51). Malignant degeneration is rare in schwannomas (32). They are also less likely to produce symptoms compared with neurofibromas, and the rate of successful surgical resection is generally higher (57).

Radiologic Features.—Schwannomas are often indistinguishable from neurofibromas at imaging (58). They often appear as round or fusiform hypoattenuating masses at CT (26). The typical signal intensity characteristics of schwannomas at MRI are similar to those of neurofibromas, with intermediate signal intensity at T1-weighted MRI (iso- to hypointense to muscle) and signal hyperintensity at T2-weighted MRI (56). Variable enhancement is seen at CT and MRI (26). In addition, schwannomas can show the target sign, although it is seen less frequently compared with neurofibromas (58). The fascicular sign is another typical imaging appearance seen in schwannomas at T2-weighted MRI, where they demonstrate numerous ringlike structures internally (59). As schwannomas age, they undergo cystic degeneration (56). This is more commonly seen in retroperitoneal schwannomas as they grow to be larger than 5 cm (Fig 8a, 8b). Long-standing schwannomas can also show calcifications and hemorrhage (26,32).

Pathologic and Molecular Features.—At gross pathologic evaluation, schwannomas are well-circumscribed encapsulated masses that display tan-yellow cut surfaces and grow eccentrically to the tumor from which they originate (51). Large long-standing tumors may undergo cystic degeneration and may show hemorrhage, necrosis, and calcification (Fig 8c) (51). Characteristic microscopic features include admixed cellular "Antoni A" and loose hypocellular "Antoni B" zones. Antoni A zones commonly exhibit *Verocay body formation*, which is defined as rows of palisading cells separated by a hypocellular hyalinized area (Fig 8d, 8e) (51). Schwannomas are strongly and diffusely S100 positive (51).

Malignant Peripheral Nerve Sheath Tumors

Epidemiologic and Clinical Features.—Malignant peripheral nerve sheath tumors (MPNSTs) are malignant soft-tissue sarcomas that arise from peripheral nerves either de novo (approximately 50%) or in a preexisting plexiform neurofibroma (54). They account for up to 10% of soft-tissue sarcomas (56). The age at onset in patients with neurofibromatosis type 1 is typically 20–30 years, and patients without neurofibromatosis type 1 tend to be older than 60 years at diagnosis (60). A small subset of MPNSTs occur in patients who have undergone prior radiation therapy (often for breast cancer or lymphoma), with an average lag time of 15 years (54,61). Presenting symptoms are usually related to the nerve or nerves involved and are similar to symptoms of neurofibroma (53). A sudden increase in size of a known neurofibroma is also suggestive of an MPNST (62). Long-term prognosis is poor because of the potential of local recurrence and metastasis (54).

Radiologic Features.—MPNSTs show heterogeneous attenuation at CT, with a higher likelihood of central necrosis and/or hemorrhage compared with benign neurogenic tumors (53). The MRI appearance is also heterogeneous, with possible regions of necrosis and/or hemorrhage (Fig 9a–9c). Among the key features that differentiate MPNST from neurofibroma include large tumor size, peripheral enhancement, perilesional edema, intralesional cysts, and

Figure 8. Schwannoma with cystic degeneration in a 41-year-old woman with a calcified abdominal mass seen on a radiograph of the lumbar spine obtained for sciatica (not shown). **(a)** Axial contrast-enhanced CT image shows a low-attenuation mass with linear and curvilinear calcifications (arrow). **(b)** Axial fat-saturated T2-weighted MR image shows the mass to be heterogeneously hyperintense, with an internal cystic formation (*). **(c)** Photograph from gross pathologic examination shows a well-circumscribed tumor with a tan-yellow solid and cystic cut surface (arrow) that is 60% white fibrous tissue and 40% yellow fatty tissue. In addition, there is a central hemorrhagic cystic component (*). **(d)** Low-power photomicrograph shows a central cyst (*) with surrounding smaller cysts (arrow). (Hematoxylin-eosin stain; original magnification, ×40.) **(e)** High-power photomicrograph shows Verocay bodies made of palisading cells (arrow) that are separated by a hypocellular hyalinized area (*). (Hematoxylin-eosin stain; original magnification, ×200.)

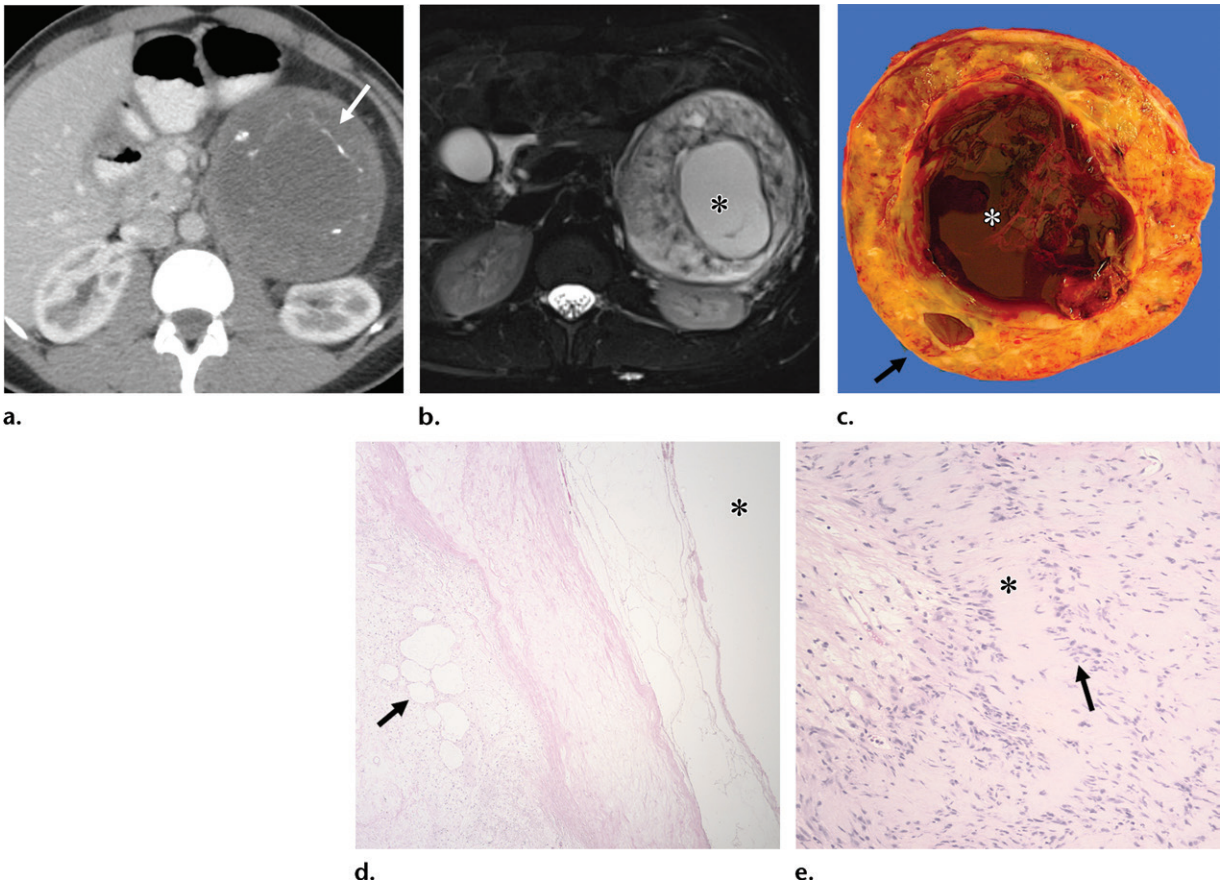

ill-defined borders (62,63). Fused fluorine 18 (^{18}F)-fluorodeoxyglucose (FDG) PET/CT can be useful for evaluation of malignant degeneration of neurofibroma to MPNST (63).

Pathologic and Molecular Features.—MPNSTs often manifest as large fusiform masses with fleshy variegated cut surfaces that display hemorrhage and/or necrosis (Fig 9d). Histologically, these tumors are variably cellular and composed of fascicles of spindle cells with tapered or wavy nuclei, indistinct cytoplasmic borders, and brisk mitotic activity (Fig 9e) (51). In cases originating from a benign nerve sheath tumor, most commonly a neurofibroma, transition areas of increased cellularity may be seen (51).

Ganglioneuromas

Epidemiologic and Clinical Features.—Ganglioneuromas are benign tumors that arise from the paravertebral sympathetic ganglia and account for 0.7%–1.6% of all primary retroperitoneal tumors (64). Internally, these tumors are composed of mature primitive neural crest cells (65). They are typically asymptomatic and manifest in children, adolescents, and young adults, with a slight female predominance (65). Ganglioneuromas can arise from maturing neuroblastomas or ganglioneuroblastomas (66). They rarely secrete sufficient amounts of catecholamines to cause sympathetic symptoms such as flushing. Complete surgical resection is curative in most patients (66).

Radiologic Features.—A ganglioneuroma typically manifests as a vertically oriented paravertebral mass in the retroperitoneum or posterior mediastinum. In the retroperitoneum, ganglioneuromas can arise from the sympathetic chain (more common) or the adrenal medulla (56,66). At CT, they manifest as a mildly hypoattenuating

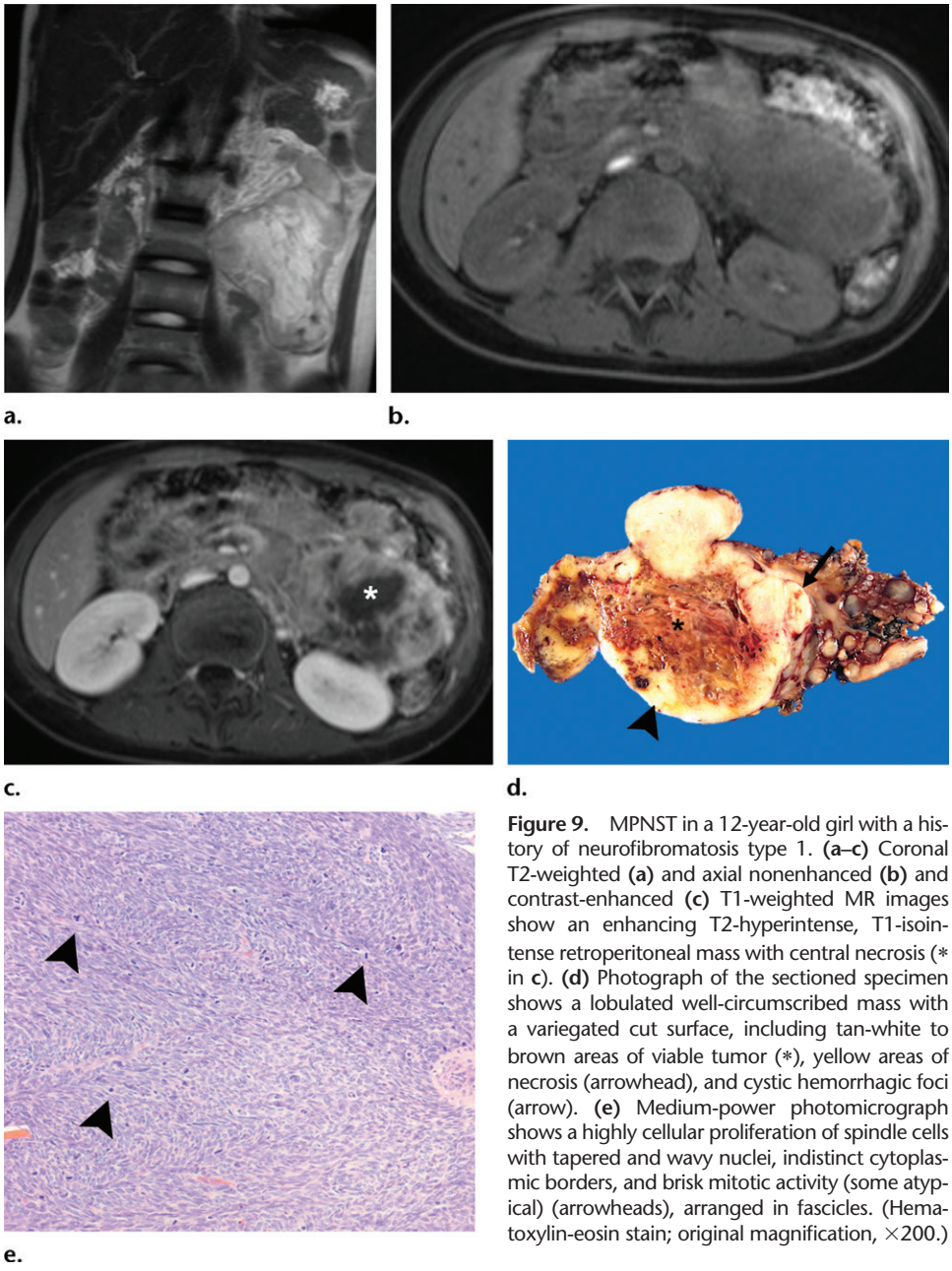

Figure 9. MPNST in a 12-year-old girl with a history of neurofibromatosis type 1. **(a–c)** Coronal T2-weighted **(a)** and axial nonenhanced **(b)** and contrast-enhanced **(c)** T1-weighted MR images show an enhancing T2-hyperintense, T1-isointense retroperitoneal mass with central necrosis (* in **c**). **(d)** Photograph of the sectioned specimen shows a lobulated well-circumscribed mass with a variegated cut surface, including tan-white to brown areas of viable tumor (*), yellow areas of necrosis (arrowhead), and cystic hemorrhagic foci (arrow). **(e)** Medium-power photomicrograph shows a highly cellular proliferation of spindle cells with tapered and wavy nuclei, indistinct cytoplasmic borders, and brisk mitotic activity (some atypical) (arrowheads), arranged in fascicles. (Hematoxylin-eosin stain; original magnification, ×200.)

well-defined homogeneous mass with variable enhancement (56). Calcifications can be seen in up to 25% of cases and are often punctate or speckled, while central necrosis and hemorrhage are rarely encountered (56,66). Heterogeneous signal intensity is seen at both T1-weighted and T2-weighted MRI, with the degree of hyperintensity at T2-weighted MRI positively correlating with the signal intensity of the myxoid stroma found in situ (67). A whorled appearance has also been described at T2-weighted MRI and manifests as internal curvilinear bands of low signal intensity (Fig 10a, 10b) (67). These are thought to represent the interlacing areas of Schwann cells and collagen fibers (Fig 10d) in a background myxoid stroma that represent the surrounding high signal intensity in the lesion at T2-weighted MRI (67). The appearance at contrast-enhanced imaging is variable; however, a lack of early enhancement has been observed, with a gradual increase during the more delayed phases (67). This has been postulated to occur because of the abundant myxoid matrix, which could result in delayed progressive accumulation of contrast material in the extracellular space (68).

Pathologic and Molecular Features.—At gross pathologic evaluation, these tumors are well-defined, with gelatinous tan-gray cut surfaces (Fig 10c). Microscopically, interlacing areas of spindled Schwann cells with bland pointed nuclei and ganglion cells intermixed with collagenous

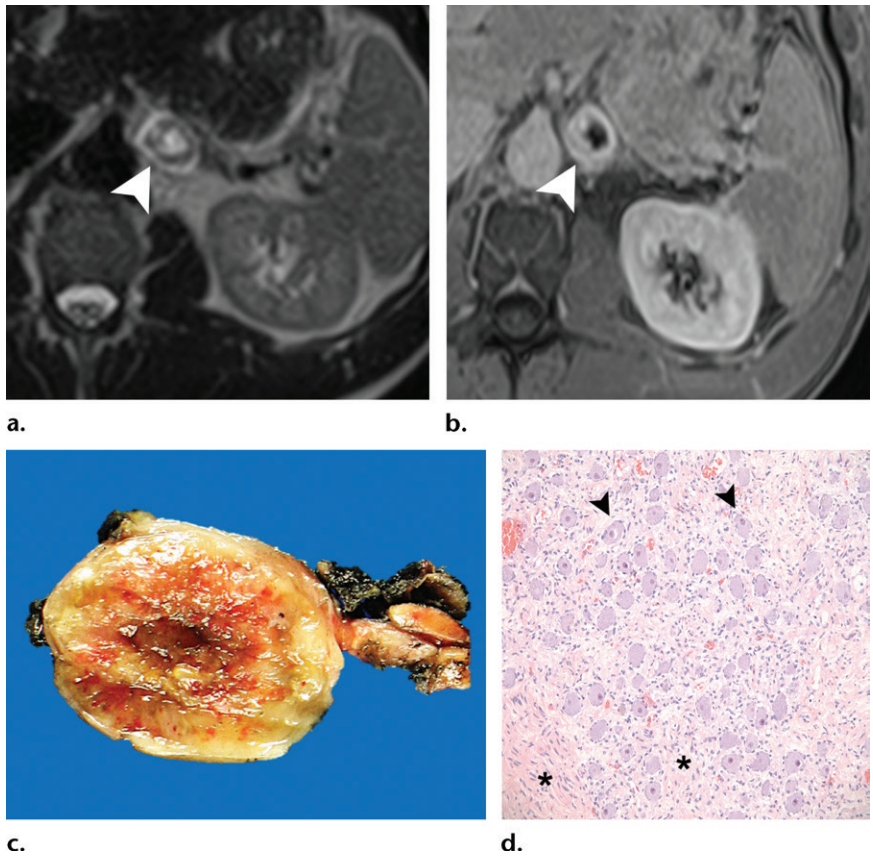

Figure 10. Ganglioneuroma in a 39-year-old man with a left suprarenal mass that was found incidentally at US (not shown). **(a)** Axial T2-weighted image shows a hyperintense mass (due to a myxoid stroma), with a curvilinear band of signal hypointensity (arrowhead), corresponding to the whorled appearance that has been described in these masses. **(b)** Axial fat-saturated contrast-enhanced T1-weighted MR image shows predominantly peripheral enhancement (arrowhead). **(c)** Photograph of the gross pathologic specimen shows a well-defined mass with a gelatinous tan-brown focally hemorrhagic cut surface. **(d)** Medium-power photomicrograph shows spindled Schwann cells (*) with bland pointed nuclei and ganglion cells (arrowheads) intermixed in a collagenous stroma. (Hematoxylin-eosin stain; original magnification, ×100.)

stroma are often seen in a background of myxoid stroma (Fig 10d). The lack of neuroblasts is key in excluding an underlying malignant neoplasm, such as ganglioneuroblastoma or neuroblastoma (51).

Ganglioneuroblastomas

Epidemiologic and Clinical Features.—Ganglioneuroblastomas are rare malignant tumors that arise from the sympathetic chain and are composed of both mature and immature ganglion cells (66). Unlike ganglioneuromas, they are most commonly seen arising from the adrenal medulla, followed by the paraspinal sympathetic chain in the retroperitoneum, and to a lesser extent, the posterior mediastinum (65). Ganglioneuroblastomas primarily affect children, with a mean age of onset of 2–4 years (66). The malignant potential of ganglioneuroblastomas is dependent on the degree of immaturity of the neural crest cells. The prognosis is generally more favorable compared with that of neuroblastomas (65).

Radiologic Features.—The CT and MRI appearances of ganglioneuroblastomas vary from solid to cystic or a combination of both solid and cystic components (66). Enhancement after administration of contrast material is also variable. (Fig E6a; a full DICOM image stack is available online.) Calcifications and necrosis or hemorrhage are more commonly present than they are with ganglioneuromas (65). Although calcification may be difficult to detect at MRI, the presence of necrosis and hemorrhage manifests as regions of signal hyperintensity at T1- and T2-weighted MRI. Avid radiotracer uptake at ^{123}I MIBG imaging is seen in approximately 70% of cases (65).

Pathologic and Molecular Features.—The gross and microscopic appearances of ganglioneuroblastomas are variable, depending on the subtype and degree of differentiation (Fig E6b, E6c). At gross pathologic evaluation, these tumors often exhibit areas of hemorrhage and/or necrosis. Microscopic features include neuroblasts, mature ganglion

cells, and Schwannian stroma. Patients who have molecular aberrations in *MYC*, *ALK,* or *ATRX* genes tend to have a worse prognosis (69–71).

Paragangliomas

Epidemiologic and Clinical Features.—Paragangliomas, also known as extra-adrenal pheochromocytomas, are rare tumors of chromaffin cell origin that arise from the extra-adrenal paraganglion cells in the sympathetic or parasympathetic chains (9). Sympathetic paragangliomas secrete catecholamine, and approximately 40% of patients with them present with clinical findings related to excess catecholamine, including hypertension and tachycardia (26). Parasympathetic paragangliomas are located in the base of the skull and neck and are associated with the branches of the glossopharyngeal and vagal nerves, whereas sympathetic paragangliomas arise anywhere along the sympathetic chain, most commonly in the abdomen (approximately 75% of all sympathetic paragangliomas) (72). Therefore, retroperitoneal paragangliomas are almost exclusively sympathetic paragangliomas (73). In the abdomen, the most common location for primary paragangliomas is in the organ of Zuckerkandl, which is located at the origin of the inferior mesenteric artery near the aortic bifurcation (26).

Paragangliomas are associated with several genetic disorders in approximately 30%–40% of cases, including multiple endocrine neoplasia syndromes and von Hippel–Lindau syndrome (39,72). The mean age at presentation of patients with paraganglioma is during the second to fourth decades of life (39). The diagnosis can be made clinically on the basis of detection of elevated metanephrine or vanillylmandelic acid levels in the urine (73). The risk of malignancy in sympathetic paragangliomas is estimated to be in the range of 30%–40% (32). Treatment usually consists of surgical resection with postoperative radiation (74,75). Preoperative medical treatment with α-adrenergic blockers is crucial to prevention of life-threatening complications secondary to intraoperative catecholamine release (75).

Radiologic Features.—Benign and malignant paragangliomas are difficult to distinguish on the basis of imaging unless tumors appear locally aggressive or metastases are present at the time of diagnosis (56). At CT, paragangliomas are typically heterogeneous, and necrosis, hemorrhage, and/or calcifications can often be seen (56). Avid contrast material enhancement is often noted because of hypervascularity, especially peripherally (Fig 11a) (26). Early concerns about the risk of a hypertensive crisis after the use of intravenous contrast material in patients with known catecholamine hypersecreting tumors have since been refuted in subsequent studies (76). At T2-weighted MRI, diffuse high signal intensity (a "lightbulb" appearance) has often been described in paragangliomas. However, a more complex appearance is frequently observed because of the signal heterogeneity that is associated with hemorrhage and/or necrosis (Fig 11b, 11c) (26). T1-weighted MRI typically shows intermediate to low signal intensity. Areas of signal hyperintensity at T1-weighted MRI may be secondary to hemorrhage (39). Signal intensity voids at T1- and T2-weighted MRI can create the typical "salt and pepper" appearance (64).

If tumor localization is not achieved or if there is a high likelihood for distant metastases, functional nuclear imaging with ^{123}I MIBG, indium 111 (^{111}In) pentetreotide, and/or PET are often performed (73). Until recently, ^{18}F-FDG PET imaging has been shown to be the most sensitive modality for diagnosis of metastatic sites of disease (32). However, recent evidence has shown that ^{68}Ga-DOTATATE PET/CT is superior to other functional and structural imaging modalities for localization and staging of paragangliomas (77).

Pathologic and Molecular Features.—At gross pathologic examination, these tumors are typically well circumscribed with myxoid and gelatinous cut surfaces (Fig 11d). Microscopic features include the characteristic zellballen growth pattern, with nests of tumor cells surrounded by fibrovascular septa (Fig 11e) (78). The tumor cells show eosinophilic granular cytoplasms, central nuclei with nucleoli, and intranuclear pseudoinclusions (Fig 11f) (78). A substantial subset of patients with paragangliomas harbor mutations in succinate dehydrogenase (79).

Skeletal Muscle Tumors

Epidemiologic and Clinical Features

Rhabdomyosarcoma (RMS) is a malignant tumor arising from primitive mesenchymal cells that show skeletal muscle differentiation (9). It is the most common soft-tissue sarcoma in children aged 15 years and younger. Nevertheless, RMS is rare in adults (80). RMS is divided into four major subtypes: *(a)* embryonal RMS (greater than 50% of all cases), *(b)* alveolar RMS, *(c)* pleomorphic RMS, and *(d)* sclerosing and spindle-cell RMS (9). The most common site of involvement is the head and neck (approximately 35% of all cases), followed by the genitourinary system (81). Approximately 7%–19% of RMSs arise in the

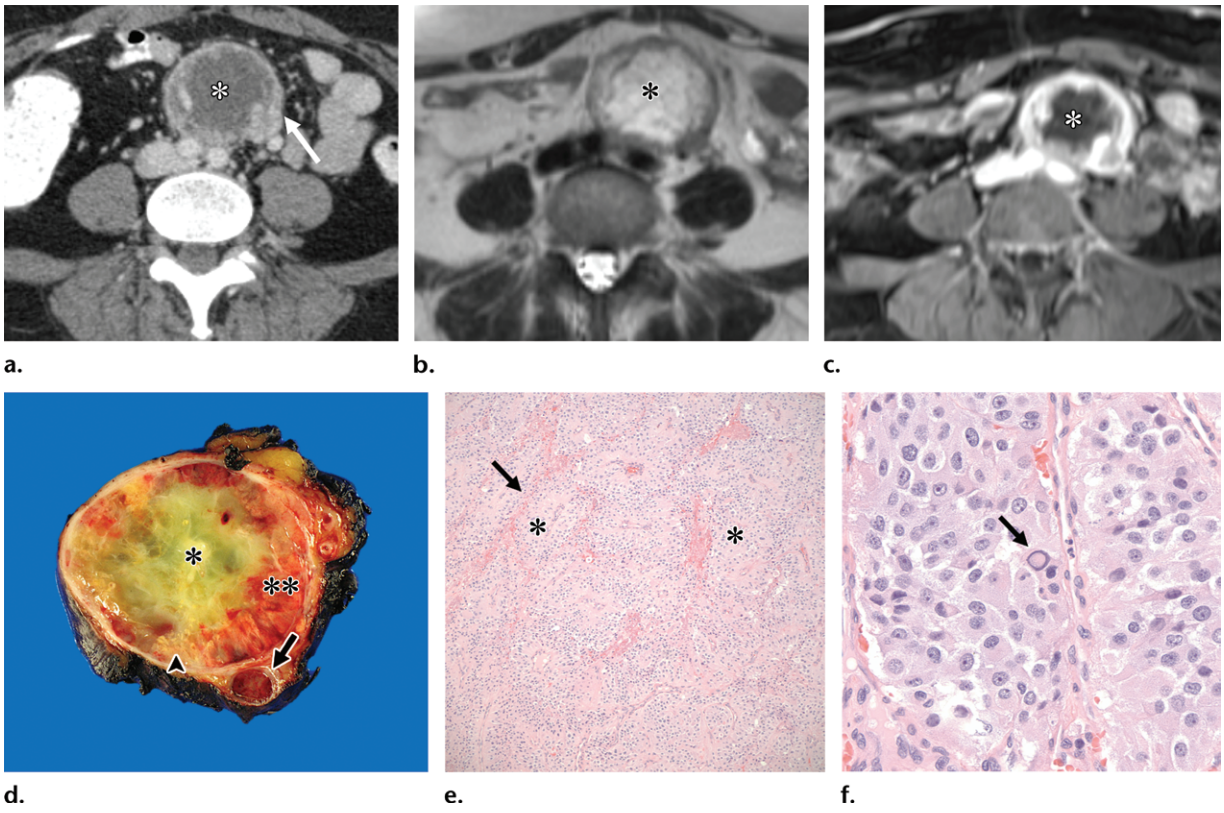

Figure 11. Paraganglioma in a 47-year-old woman who presented with weight loss, abdominal pain, and sciatica. **(a)** Axial contrast-enhanced CT image shows a large mass at the level of the aortic bifurcation, with central necrosis (*) and avid peripheral enhancement (arrow). **(b, c)** Axial T2-weighted **(b)** and contrast-enhanced T1-weighted **(c)** MR images also show the central necrosis (*) and the avid peripheral enhancement. **(d)** Photograph at gross pathologic examination shows a well-circumscribed and encapsulated mass with a myxoid and gelatinous central component (*) and surrounding red hemorrhagic (**) and yellow necrotic (arrowhead) foci. A large-caliber vessel (inferior mesenteric artery) is completely occluded by the tumor (arrow). **(e)** Low-power photomicrograph shows the characteristic zellballen growth pattern with nests of tumor cells (*) surrounded by fibrovascular septa (arrow). (Hematoxylin-eosin stain; original magnification, ×40.) **(f)** High-power photomicrograph shows the eosinophilic granular cell cytoplasm, the central nuclei with nucleoli, and intranuclear pseudoinclusions (arrow). (Hematoxylin-eosin stain; original magnification, ×400.)

retroperitoneum (82). In terms of risk stratification and prognostication, the retroperitoneum is considered an unfavorable primary site (81).

Radiologic Features

Retroperitoneal RMS can manifest as well-circumscribed lesions or show an infiltrative or invasive appearance at the time of diagnosis (83). At CT, they are typically heterogeneously attenuating, with central low attenuation that is secondary to necrosis (83). Enhancement with contrast material is also heterogeneous, especially when there is central necrosis (Fig E7a; a full DICOM image stack is available online.) They usually show signal hypo- to isointensity at T1-weighted MRI and iso- to hyperintensity at T2-weighted MRI (84). RMS is intensely avid at ^{18}F-FDG PET/CT (81).

Pathologic and Molecular Features

At gross pathologic examination, RMS can be well defined or poorly circumscribed and can occasionally exhibit necrosis and/or hemorrhage (Fig E7b). Skeletal differentiation can be defined by means of morphologic, immunohistochemical, ultrastructural, or molecular assessment. The hallmark microscopic features of embryonal RMS includes its "marbled" appearance due to variations in cellularity, with perivascular tumor cell condensation (Fig E7c) and the various stages of skeletal muscle embryogenesis commonly exhibited by the primitive mesenchymal cells (85). The rhabdomyoblasts in embryonal RMS are ovoid to spindled, contain scant to abundant eosinophilic cytoplasms, and are arranged in patternless sheets (Fig E7d) (85). Alveolar RMS is derived from the alveolar pattern that is seen histologically. Alveolar RMS is typically composed of small blue round lymphoma-like cells (85).

Miscellaneous Tumors

Undifferentiated Pleomorphic Sarcoma

Epidemiologic and Clinical Features.—Undifferentiated pleomorphic sarcoma replaced the outdated

malignant fibrous histiocytoma in the 2002 WHO classification (86). Undifferentiated pleomorphic sarcomas are commonly seen in patients during their fifth to seventh decades of life, with a higher incidence in men (87). They most frequently occur in the extremities, followed by the retroperitoneum, and are rarely seen in the peritoneal cavity of the abdomen (87). Undifferentiated pleomorphic sarcoma is a clinically aggressive tumor, with an estimated local recurrence rate of 19%–31%, and metastases are seen in 31%–35% of cases (87).

Radiologic Features.—Undifferentiated pleomorphic sarcoma has a nonspecific imaging appearance and commonly manifests as a well-defined heterogeneous mass with areas of avid contrast material enhancement at CT and MRI (Fig E8a) (88). They usually show attenuation similar to that of muscle at CT, intermediate signal intensity at T1-weighted MRI, and signal hyperintensity at T2-weighted MRI (53). The presence of hemorrhage can result in areas of signal hyperintensity at T1-weighted MRI. Calcifications are seen in 5%–20% of cases (53).

Pathologic and Molecular Features.—Undifferentiated pleomorphic sarcoma is a diagnosis made after the exclusion of differentiated pleomorphic sarcoma (eg, liposarcoma, leiomyosarcoma), and thus, extensive tumor sampling is critical for accurate tumor classification (86). At gross pathologic examination, these tumors display heterogeneous firm to fleshy cut surfaces that commonly show hemorrhage and/or necrosis (Fig E8b). Microscopically, undifferentiated pleomorphic sarcomas are hypercellular and are composed of markedly atypical cells, without evidence of lineage-specific differentiation (Fig E8c) (28).

Alveolar Soft-part Sarcoma

Epidemiologic Features.—Alveolar soft-part sarcoma (ASPS) is a rare malignant soft-tissue tumor that accounts for up to 1% of all soft-tissue sarcomas (89,90). The median age at diagnosis is 22–26 years with a higher incidence in women, especially in younger patients (89,90). ASPS most commonly occurs in the extremities in adults, whereas the head and neck are the primary sites in children (91). Approximately 3%–8% of ASPSs occur in the retroperitoneum (89,90). ASPS typically manifests as a painless slow-growing tumor. Despite its early indolent course, many ASPSs metastasize later in the disease course. Portera et al (90) reported a metastatic rate of up to 65%. The prognosis is highly dependent on the presence of metastatic disease (89). In one study (89), the overall median survival rate was 11 years in patients without metastasis and 3 years in patients with metastasis.

Radiologic Features.—The imaging appearance of ASPS reflects its rich hypervascularity. At CT, it typically manifests as a well-defined lesion that is iso- to hypoattenuating compared with muscle, with marked hypervascularity with the administration of contrast material (Fig E9a; a full DICOM image stack is available online) (92). At T1-weighted MRI, they are usually isointense compared with muscle, although they occasionally may show mild hyperintensity due to hemorrhage (92). A key imaging clue is the presence of flow voids at T1- and T2-weighted MRI (93). One recent study (93) reported that the presence of greater than five peritumoral and intratumoral flow voids in a deep soft-tissue solid enhancing lesion is diagnostic of ASPS, with sensitivity of 96% and specificity of 91%. Central necrosis has also been reported and is especially seen in larger lesions (93).

Occasionally, ASPS and other hypervascular tumors such as solitary fibrous tumors may be confused with hemangiomas, given their intense contrast material enhancement. Some of the distinguishing clues that suggest hemangiomas include their lobulated appearance, high signal intensity at T2-weighted MRI, gradual pooling of contrast material, and the presence of intralesional fat and phleboliths, which may be calcified at CT (92). Confirmation can be obtained with tagged technetium 99m red blood cell scintigraphy, if findings at cross-sectional imaging are indeterminate (94).

Pathologic and Molecular Features.—At gross pathologic examination, ASPS demonstrates rubbery tan cut surfaces with hemorrhage and/or necrosis (Fig E9b). At histologic evaluation, these tumors display a nested architecture, with lobules of tumor cells separated by delicate fibrovascular septa (95). At cytologic evaluation, tumor cells are discohesive and polygonal, with prominent nucleoli and an eosinophilic granular cytoplasm (Fig E9c). Most cases show intracytoplasmic crystalline inclusions that can be highlighted by using periodic acid Schiff diastase stain (Fig E9d). ASPS is characterized by t(X:17) translocation, resulting in fusion of the *ASPSCR1* and *TFE3* genes (95).

Cystic Tumors

Primary retroperitoneal cystic neoplasms are uncommon, with a reported incidence of one in 100 000 in adults (96). They can be broadly categorized as cysts of epithelial origin (eg, primary mucinous cystadenoma), mesothelial origin (eg,

cystic mesothelioma), or germ cell origin (eg, cystic teratoma) (26). Additional miscellaneous entities include tailgut cysts, lymphatic malformations, epidermoid cysts and pseudomyxoma retroperitonei (26). On rare occasions, solid retroperitoneal masses (such as paragangliomas) may manifest as cystic lesions (66).

Tailgut Cyst

Epidemiologic and Clinical Features.—Tailgut cysts (also known as retrorectal cystic hamartomas) are uncommon congenital lesions that arise from the embryonic hindgut (97). In one literature review (97) of 53 cases of tailgut cysts, the average age of patients at presentation was 35 years (range, 4 days to 73 years), and they occur more often in women (3:1 female-to-male ratio). Approximately half of all lesions are detected incidentally in patients with reported symptoms including low back or rectal pain, rectal fullness, and pain during defecation (97). Surgical excision is usually recommended because of the risks of malignant degeneration and infection associated with biopsy (98). Although malignant degeneration is uncommon, one literature review (98) spanning all reported cases from 1932 to 2011 reported a malignancy rate of 14%, with some subtypes including mucinous adenocarcinoma, carcinoid tumors, and squamous carcinoma.

Radiologic Features.—Tailgut cysts are characteristically located in the presacral or retrorectal space, with occasional extension into the ischioanal fossa (99). At CT, the mass typically manifests as a well-defined unilocular or multilocular hypoattenuating cystic lesion with variably thick septa and occasional calcifications (26,99). The MRI appearance mirrors the CT findings, with the cystic content appearing T2 hyperintense and T1 hypointense (Fig 12a, 12b), although signal intensity may be variable in the presence of internal hemorrhagic and/or proteinaceous debris. If septa are present, they typically show mild enhancement. Imaging findings that suggest superimposed infection or malignancy include indistinct margins, nodular wall thickening with enhancement, intracystic enhancing nodules, superior extension above S3, and/or lymphadenopathy (99).

Pathologic and Molecular Features.—Tailgut cysts are typically thin-walled multiloculated cysts that contain clear serous or opaque mucoid fluid (Fig 12c). Histologically, tailgut cysts are lined by gastrointestinal tract mucosa that is most commonly stratified squamous epithelium. (Fig 12d) (97). The underlying fibroconnective tissue may contain disorganized smooth muscle bundles; however, a well-defined muscle layer and nerve plexus are characteristically absent (97).

Lymphatic Malformation

Epidemiologic and Clinical Features.—Lymphatic malformation (also known as cystic lymphangioma), is a benign cystic mass comprising dilated lymphatic channels, which forms secondary to failure of normal lymphatic channel communication or drainage (100). They are considered a form of slow-flowing vascular malformation (101). Lymphatic malformations can occur in patients of any age, but most of them manifest in early childhood. They are most commonly found in the head or neck and are rarely encountered in the abdomen (101). They can be asymptomatic or may be associated with vague abdominal discomfort. Treatment typically includes percutaneous sclerotherapy and/or surgery (102,103).

Radiologic Features.—Because most lymphatic malformations manifest in patients during childhood, initial imaging assessment is often performed with US, which often shows a multiloculated anechoic mass with thin septa. Vascularity can occasionally be seen in the septa (101). At CT, lymphatic malformations often appear as a uniformly cystic mass and exhibit attenuation that is near that of water. The walls and/or septa are rarely perceptible, and septal enhancement is difficult to appreciate at CT. They classically can involve more than one retroperitoneal compartment and can appear as an elongated and insinuating mass, which is an important imaging clue (100). Uncomplicated lymphatic malformations usually appear as multilocular multiseptated fluid-filled masses with classic fluid high signal intensity at T2-weighted MRI and enhancing thin septa with administration of contrast material (Fig 13a, 13b). The presence of fluid-fluid levels at T2-weighted MRI may indicate hemorrhage. Signal hyperintensity at T1-weighted MRI can also be suggestive of the presence of proteinaceous or hemorrhagic debris secondary to superinfection or hemorrhage (102). One study (104) suggested that the detection of intracystic lipid through chemical shift MRI may be valuable for detection of lymphatic malformations with chylous content.

Pathologic and Molecular Features.—Lymphatic malformations have a variable appearance at gross pathologic evaluation. These lesions are typically smooth-walled and uni- or multiloculated and contain clear serous fluid (Fig 13c). Microscopic features include cystic walls composed of fibrous tissue and lined by a monolayer of endothelial cells (Fig 13d).

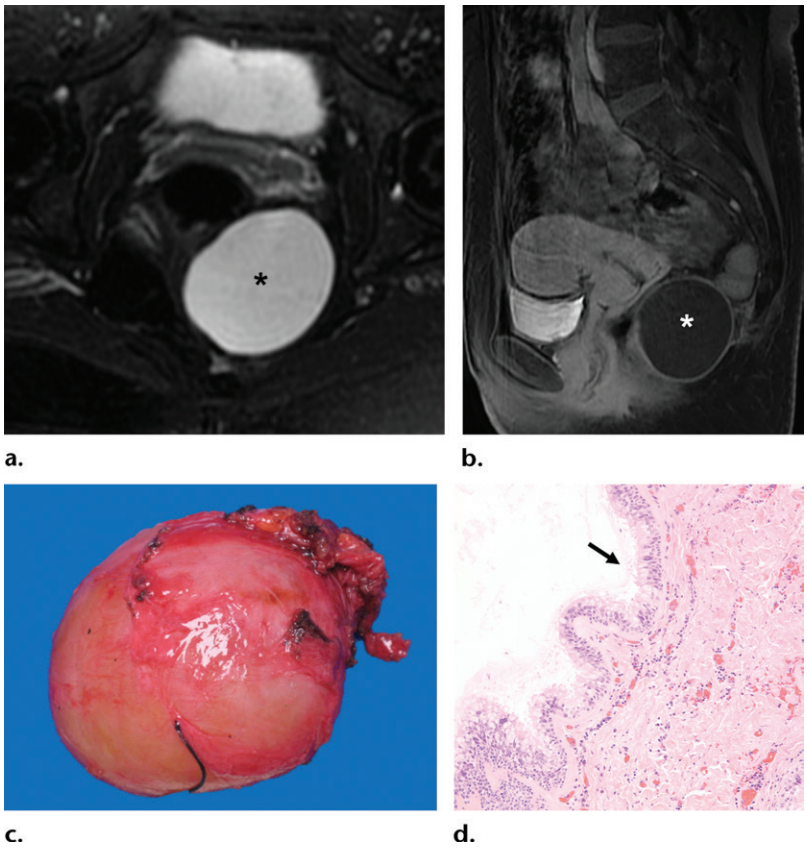

Figure 12. Tailgut cyst in a 51-year-old woman who presented with rectal discomfort. **(a, b)** Axial fat-suppressed T2-weighted **(a)** and sagittal fat-suppressed contrast-enhanced T1-weighted **(b)** MR images show a large cystic presacral mass without internal nodularity or septa (*). **(c)** Photograph at gross pathologic examination shows a cyst with a tan smooth glistening surface. **(d)** Medium-power photomicrograph shows a tailgut cyst lined by mucinous columnar epithelium (arrow) and containing serous luminal fluid. (Hematoxylin-eosin stain; original magnification, ×100.)

Algorithmic Approach

After localizing the tumor to the retroperitoneum, the radiologist should categorize the lesion as predominantly solid or cystic (Fig E1), with the caveat that certain solid masses may have internal cystic components, which often represent necrosis and/or hemorrhage. If the mass is determined to have a predominantly solid appearance, it should be scrupulously examined for the presence of macroscopic lipid because it is highly suggestive of liposarcoma. Primary retroperitoneal lipomas are uncommon and are often evaluated as well-differentiated liposarcomas, particularly in the presence of thickened septa and soft-tissue nodular components larger than or equal to 1 cm. In rare cases, a primary retroperitoneal teratoma manifests as a fat- and calcium-containing mass, possibly with a fat-fluid level. Differentiating among the different histologic categories of liposarcoma can be challenging, and a paucity of macroscopic lipid is often seen with myxoid and pleomorphic liposarcomas, with the former also exhibiting a myxoid matrix (T2-hyperintense components with a low level of enhancement). Because well-differentiated liposarcomas do not metastasize, the presence of distant disease is suggestive of a more aggressive higher-grade tumor.

If no macroscopic lipid is detected, the relationship of the lesion to adjacent vessels should be assessed. If there is evidence of vessel invasion, then the possibility of leiomyosarcoma should be strongly considered. However, because the majority of leiomyosarcomas are classified as extravascular, vessel invasion is not always visible radiologically. If no vessel invasion is seen, the predominant signal intensity of the mass at T2-weighted MRI should be assessed. The presence of a target sign of peripheral signal hyperintensity and central hypointensity at T2-weighted MRI is suggestive of a neurogenic origin. A predominant T2-hyperintense mass with brisk hypervascular enhancement can be seen in paragangliomas, while a paucity of enhancement is suggestive of an underlying myxoid matrix that can be seen with a schwannoma, neurofibroma, myxoid liposarcoma with no detectable fat, or low-grade myxofibrosarcoma. Signal hypointensity at T2-weighted MRI is uncommon but should raise

Figure 13. Lymphatic malformation in a 17-year-old adolescent girl with left-sided flank pain. **(a, b)** Axial T2-weighted **(a)** and contrast-enhanced T1-weighted **(b)** images show a multiseptated cystic mass (*) with mild septal enhancement (arrow in **b**). **(c)** Photograph at gross pathologic examination of the specimen reveals a smooth-walled multiloculated cystic structure (*) filled with a small amount of clear serous fluid. No definitive excrescences are identified, and minimal solid components are seen. **(d)** Low-power photomicrograph shows cystic channels lined by a monolayer of endothelial cells (arrow), overlying fibrous tissue with lymphocytic infiltration (*). (Hematoxylin-eosin stain; original magnification, ×100.)

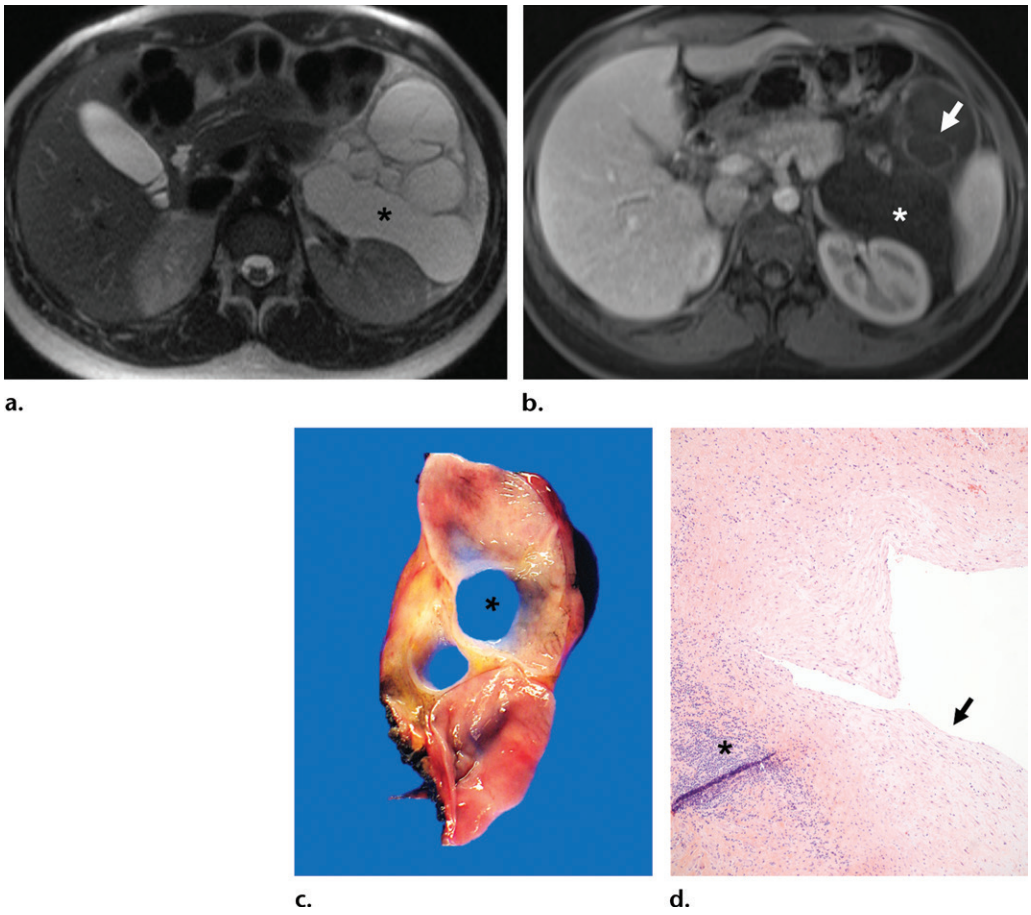

the possibility of a leiomyoma, particularly if the patient is a woman with a history of fibroids. Heterogeneous signal intensity at T2-weighted MRI is more common and can be seen with a plethora of neoplasms that are difficult to confidently distinguish on the basis of imaging alone. If the lesion is paravertebral, the possibility of a neurogenic tumor such as a ganglioneuroma or ganglioneuroblastoma could be considered, with the former characterized by a whorled appearance at T2-weighted MRI.

Cystic retroperitoneal neoplasms are challenging to distinguish on the basis of imaging alone. If the mass occupies more than one retroperitoneal compartment and/or insinuates between structures without invading them, then the possibility of a lymphatic malformation should be strongly considered. Cystic teratomas are rare and may manifest with a fat-fluid level. A tailgut cyst or retrorectal hamartoma should be included in the differential diagnosis of any cystic mass located in the presacral space.

It is important to evaluate the abdominopelvic cavity carefully for any abnormalities outside of the retroperitoneum that may suggest an alternate diagnosis, specifically lymphoma or metastatic disease. Lymphoma is the most common retroperitoneal malignancy, accounting for up to one-third of all cases (2). Retroperitoneal lymphoma is seen in 25%–55% of cases of lymphoma, most commonly manifesting as well-defined para-aortic or pelvic masses (lymph nodes) with homogeneous enhancement and no necrosis or calcification when imaged before treatment. The adenopathy may be discrete or may form a conglomerate nodal mass. In some cases, lymphoma may appear infiltrative, with a mantlelike growth pattern, typically around the major vessels (52).

If the patient has a history of primary malignancy or if there are imaging findings suggestive of a primary malignancy elsewhere (eg, a concurrent renal mass or the presence of skeletal metastatic disease), retroperitoneal metastatic lymphadenopathy should be strongly considered. This is typically

seen in patients with renal cell carcinoma, cervical cancer, and prostate cancer (52). In addition, patients with primary malignant testicular neoplasms can develop metastatic retroperitoneal disease, which sometimes occurs in the absence of an apparent gonadal primary tumor (105).

Conclusion

Primary retroperitoneal neoplasms are a rare and eclectic group of tumors with a variety of imaging features, some of which can be derived from their histologic appearance. Incorporating a systematic approach to these neoplasms, taking into account epidemiologic and clinical features, allows the radiologist to provide consistently high-quality accurate interpretations for referring providers. Accurate interpretation is critical because it allows the radiologist to help direct the next step in managing patient care, whether it is conservative or surgical, and can help to guide referring providers before potential biopsy (ie, to sample a higher-grade component of the neoplasm). An understanding of the expected gross pathologic and microscopic appearance of these lesions can help facilitate these radiologic interpretations.

Acknowledgment.—The authors would like to thank Mark Saba, MA, senior designer and illustrator, User Experience and Design Services, Yale University, Information Technology Services, for creating the illustrations in Figure 1.

References

1. Armstrong JR, Cohn I Jr. Primary malignant retroperitoneal tumors. Am J Surg 1965;110(6):937–943.
2. Felix EL, Wood DK, Das Gupta TK. Tumors of the retroperitoneum. Curr Probl Cancer 1981;6(1):1–47.
3. Tirkes T, Sandrasegaran K, Patel AA, et al. Peritoneal and retroperitoneal anatomy and its relevance for cross-sectional imaging. RadioGraphics 2012;32(2):437–451.
4. Molmenti EP, Balfe DM, Kanterman RY, Bennett HF. Anatomy of the retroperitoneum: observations of the distribution of pathologic fluid collections. Radiology 1996;200(1):95–103.
5. Osman S, Lehnert BE, Elojeimy S, et al. A comprehensive review of the retroperitoneal anatomy, neoplasms, and pattern of disease spread. Curr Probl Diagn Radiol 2013;42(5):191–208.
6. Ishikawa K, Tohira H, Mizushima Y, Matsuoka T, Mizobata Y, Yokota J. Traumatic retroperitoneal hematoma spreads through the interfascial planes. J Trauma 2005;59(3):595–607; discussion 607–608.
7. Aizenstein RI, Wilbur AC, O'Neil HK. Interfascial and perinephric pathways in the spread of retroperitoneal disease: refined concepts based on CT observations. AJR Am J Roentgenol 1997;168(3):639–643.
8. Nishino M, Hayakawa K, Minami M, Yamamoto A, Ueda H, Takasu K. Primary retroperitoneal neoplasms: CT and MR imaging findings with anatomic and pathologic diagnostic clues. RadioGraphics 2003;23(1):45–57.
9. Fletcher CDM; World Health Organization. International Agency for Research on Cancer. WHO classification of tumours of soft tissue and bone. 4th ed. Lyon, France: IARC, 2013.
10. Murphey MD, Arcara LK, Fanburg-Smith J. From the archives of the AFIP: imaging of musculoskeletal liposarcoma with radiologic-pathologic correlation. RadioGraphics 2005;25(5):1371–1395.
11. Knebel C, Neumann J, Schwaiger BJ, et al. Differentiating atypical lipomatous tumors from lipomas with magnetic resonance imaging: a comparison with MDM2 gene amplification status. BMC Cancer 2019;19(1):309.
12. Craig WD, Fanburg-Smith JC, Henry LR, Guerrero R, Barton JH. Fat-containing lesions of the retroperitoneum: radiologic-pathologic correlation. RadioGraphics 2009;29(1):261–290.
13. Gupta P, Potti TA, Wuertzer SD, Lenchik L, Pacholke DA. Spectrum of Fat-containing Soft-Tissue Masses at MR Imaging: The Common, the Uncommon, the Characteristic, and the Sometimes Confusing. RadioGraphics 2016;36(3):753–766.
14. Shaaban AM, Rezvani M, Tubay M, Elsayes KM, Woodward PJ, Menias CO. Fat-containing Retroperitoneal Lesions: Imaging Characteristics, Localization, and Differential Diagnosis. RadioGraphics 2016;36(3):710–734.
15. Singer S, Antonescu CR, Riedel E, Brennan MF. Histologic subtype and margin of resection predict pattern of recurrence and survival for retroperitoneal liposarcoma. Ann Surg 2003;238(3):358–370; discussion 370–371.
16. Kransdorf MJ. Malignant soft-tissue tumors in a large referral population: distribution of diagnoses by age, sex, and location. AJR Am J Roentgenol 1995;164(1):129–134.
17. Goldblum JR, Folpe AL, Weiss SW, Enzinger FM, Weiss SW. Enzinger and Weiss's soft tissue tumors. 6th ed. Philadelphia, Pa: Saunders/Elsevier, 2014.
18. Johnson CN, Ha AS, Chen E, Davidson D. Lipomatous Soft-tissue Tumors. J Am Acad Orthop Surg 2018;26(22):779–788.
19. Dalal KM, Kattan MW, Antonescu CR, Brennan MF, Singer S. Subtype specific prognostic nomogram for patients with primary liposarcoma of the retroperitoneum, extremity, or trunk. Ann Surg 2006;244(3):381–391.
20. Dalal KM, Antonescu CR, Singer S. Diagnosis and management of lipomatous tumors. J Surg Oncol 2008;97(4):298–313.
21. Antonescu CR, Tschernyavsky SJ, Decuseara R, et al. Prognostic impact of P53 status, TLS-CHOP fusion transcript structure, and histological grade in myxoid liposarcoma: a molecular and clinicopathologic study of 82 cases. Clin Cancer Res 2001;7(12):3977–3987.
22. Downes KA, Goldblum JR, Montgomery EA, Fisher C. Pleomorphic liposarcoma: a clinicopathologic analysis of 19 cases. Mod Pathol 2001;14(3):179–184.
23. Brisson M, Kashima T, Delaney D, et al. MRI characteristics of lipoma and atypical lipomatous tumor/well-differentiated liposarcoma: retrospective comparison with histology and MDM2 gene amplification. Skeletal Radiol 2013;42(5):635–647.
24. Kransdorf MJ, Bancroft LW, Peterson JJ, Murphey MD, Foster WC, Temple HT. Imaging of fatty tumors: distinction of lipoma and well-differentiated liposarcoma. Radiology 2002;224(1):99–104.
25. Hong SH, Kim KA, Woo OH, et al. Dedifferentiated liposarcoma of retroperitoneum: spectrum of imaging findings in 15 patients. Clin Imaging 2010;34(3):203–210.
26. Rajiah P, Sinha R, Cuevas C, Dubinsky TJ, Bush WH Jr, Kolokythas O. Imaging of uncommon retroperitoneal masses. RadioGraphics 2011;31(4):949–976.
27. Thway K. Well-differentiated liposarcoma and dedifferentiated liposarcoma: an updated review. Semin Diagn Pathol 2019;36(2):112–121.
28. Hornick JL. Subclassification of pleomorphic sarcomas: How and why should we care? Ann Diagn Pathol 2018;37:118–124.
29. Weaver J, Downs-Kelly E, Goldblum JR, et al. Fluorescence in situ hybridization for MDM2 gene amplification as a diagnostic tool in lipomatous neoplasms. Mod Pathol 2008;21(8):943–949.
30. Lee ATJ, Thway K, Huang PH, Jones RL. Clinical and Molecular Spectrum of Liposarcoma. J Clin Oncol 2018;36(2):151–159.
31. Hornick JL, Bosenberg MW, Mentzel T, McMenamin ME, Oliveira AM, Fletcher CD. Pleomorphic liposarcoma: clinicopathologic analysis of 57 cases. Am J Surg Pathol 2004;28(10):1257–1267.

32. Shanbhogue AK, Fasih N, Macdonald DB, Sheikh AM, Menias CO, Prasad SR. Uncommon primary pelvic retroperitoneal masses in adults: a pattern-based imaging approach. RadioGraphics 2012;32(3):795–817.
33. Billings SD, Folpe AL, Weiss SW. Do leiomyomas of deep soft tissue exist? an analysis of highly differentiated smooth muscle tumors of deep soft tissue supporting two distinct subtypes. Am J Surg Pathol 2001;25(9):1134–1142.
34. Paal E, Miettinen M. Retroperitoneal leiomyomas: a clinicopathologic and immunohistochemical study of 56 cases with a comparison to retroperitoneal leiomyosarcomas. Am J Surg Pathol 2001;25(11):1355–1363.
35. Fasih N, Prasad Shanbhogue AK, Macdonald DB, et al. Leiomyomas beyond the uterus: unusual locations, rare manifestations. RadioGraphics 2008;28(7):1931–1948.
36. Wile AG, Evans HL, Romsdahl MM. Leiomyosarcoma of soft tissue: a clinicopathologic study. Cancer 1981;48(4):1022–1032.
37. Adam YG, Oland J, Halevy A, Reif R. Primary retroperitoneal soft-tissue sarcomas. J Surg Oncol 1984;25(1):8–11.
38. Hartman DS, Hayes WS, Choyke PL, Tibbetts GP. From the archives of the AFIP. Leiomyosarcoma of the retroperitoneum and inferior vena cava: radiologic-pathologic correlation. RadioGraphics 1992;12(6):1203–1220.
39. Marko J, Wolfman DJ. Retroperitoneal Leiomyosarcoma From the Radiologic Pathology Archives. RadioGraphics 2018;38(5):1403–1420.
40. Strauss DC, Hayes AJ, Thway K, Moskovic EC, Fisher C, Thomas JM. Surgical management of primary retroperitoneal sarcoma. Br J Surg 2010;97(5):698–706.
41. Cooley CL, Jagannathan JP, Kurra V, et al. Imaging features and metastatic pattern of non-IVC retroperitoneal leiomyosarcomas: are they different from IVC leiomyosarcomas? J Comput Assist Tomogr 2014;38(5):687–692.
42. Penel N, Amela EY, Decanter G, Robin YM, Marec-Berard P. Solitary fibrous tumors and so-called hemangiopericytoma. Sarcoma 2012;2012:690251.
43. Sun J, Yu XR, Shi BB, Zheng J, Wu JT. CT features of retroperitoneal solitary fibrous tumor: report of three cases and review of the literature. World J Surg Oncol 2014;12(1):324.
44. Keraliya AR, Tirumani SH, Shinagare AB, Zaheer A, Ramaiya NH. Solitary Fibrous Tumors: 2016 Imaging Update. Radiol Clin North Am 2016;54(3):565–579.
45. Insabato L, Siano M, Somma A, Gentile R, Santangelo M, Pettinato G. Extrapleural solitary fibrous tumor: a clinicopathologic study of 19 cases. Int J Surg Pathol 2009;17(3):250–254.
46. Thway K, Ng W, Noujaim J, Jones RL, Fisher C. The Current Status of Solitary Fibrous Tumor: Diagnostic Features, Variants, and Genetics. Int J Surg Pathol 2016;24(4):281–292.
47. Rajeev R, Patel M, Jayakrishnan TT, et al. Retroperitoneal solitary fibrous tumor: surgery as first line therapy. Clin Sarcoma Res 2015;5(1):19.
48. Sanfilippo R, Miceli R, Grosso F, et al. Myxofibrosarcoma: prognostic factors and survival in a series of patients treated at a single institution. Ann Surg Oncol 2011;18(3):720–725.
49. Petscavage-Thomas JM, Walker EA, Logie CI, Clarke LE, Duryea DM, Murphey MD. Soft-tissue myxomatous lesions: review of salient imaging features with pathologic comparison. RadioGraphics 2014;34(4):964–980.
50. Lefkowitz RA, Landa J, Hwang S, et al. Myxofibrosarcoma: prevalence and diagnostic value of the "tail sign" on magnetic resonance imaging. Skeletal Radiol 2013;42(6):809–818.
51. Skovronsky DM, Oberholtzer JC. Pathologic classification of peripheral nerve tumors. Neurosurg Clin N Am 2004;15(2):157–166.
52. Scali EP, Chandler TM, Heffernan EJ, Coyle J, Harris AC, Chang SD. Primary retroperitoneal masses: what is the differential diagnosis? Abdom Imaging 2015;40(6):1887–1903.
53. Murphey MD, Smith WS, Smith SE, Kransdorf MJ, Temple HT. From the archives of the AFIP. Imaging of musculoskeletal neurogenic tumors: radiologic-pathologic correlation. RadioGraphics 1999;19(5):1253–1280.
54. Perrin RG, Guha A. Malignant peripheral nerve sheath tumors. Neurosurg Clin N Am 2004;15(2):203–216.
55. Banks KP. The target sign: extremity. Radiology 2005;234(3):899–900.
56. Goenka AH, Shah SN, Remer EM. Imaging of the retroperitoneum. Radiol Clin North Am 2012;50(2):333–355, vii.
57. Kim DH, Murovic JA, Tiel RL, Kline DG. Operative outcomes of 546 Louisiana State University Health Sciences Center peripheral nerve tumors. Neurosurg Clin N Am 2004;15(2):177–192.
58. Wu JS, Hochman MG. Soft-tissue tumors and tumor-like lesions: a systematic imaging approach. Radiology 2009;253(2):297–316.
59. Stramare R, Beltrame V, Gazzola M, et al. Imaging of soft-tissue tumors. J Magn Reson Imaging 2013;37(4):791–804.
60. Evans DG, Baser ME, McGaughran J, Sharif S, Howard E, Moran A. Malignant peripheral nerve sheath tumours in neurofibromatosis 1. J Med Genet 2002;39(5):311–314.
61. Farid M, Demicco EG, Garcia R, et al. Malignant peripheral nerve sheath tumors. Oncologist 2014;19(2):193–201.
62. Pilavaki M, Chourmouzi D, Kiziridou A, Skordalaki A, Zarampoukas T, Drevelengas A. Imaging of peripheral nerve sheath tumors with pathologic correlation: pictorial review. Eur J Radiol 2004;52(3):229–239.
63. Patel NB, Stacy GS. Musculoskeletal manifestations of neurofibromatosis type 1. AJR Am J Roentgenol 2012;199(1):W99–W106.
64. Lee KY, Oh YW, Noh HJ, et al. Extraadrenal paragangliomas of the body: imaging features. AJR Am J Roentgenol 2006;187(2):492–504.
65. Lonergan GJ, Schwab CM, Suarez ES, Carlson CL. Neuroblastoma, ganglioneuroblastoma, and ganglioneuroma: radiologic-pathologic correlation. RadioGraphics 2002;22(4):911–934.
66. Rha SE, Byun JY, Jung SE, Chun HJ, Lee HG, Lee JM. Neurogenic tumors in the abdomen: tumor types and imaging characteristics. RadioGraphics 2003;23(1):29–43.
67. Zhang Y, Nishimura H, Kato S, et al. MRI of ganglioneuroma: histologic correlation study. J Comput Assist Tomogr 2001;25(4):617–623.
68. Ichikawa T, Ohtomo K, Araki T, et al. Ganglioneuroma: computed tomography and magnetic resonance features. Br J Radiol 1996;69(818):114–121.
69. Duijkers FA, Gaal J, Meijerink JP, et al. High anaplastic lymphoma kinase immunohistochemical staining in neuroblastoma and ganglioneuroblastoma is an independent predictor of poor outcome. Am J Pathol 2012;180(3):1223–1231.
70. Goto S, Umehara S, Gerbing RB, et al. Histopathology (International Neuroblastoma Pathology Classification) and MYCN status in patients with peripheral neuroblastic tumors: a report from the Children's Cancer Group. Cancer 2001;92(10):2699–2708.
71. Cheung NK, Zhang J, Lu C, et al. Association of age at diagnosis and genetic mutations in patients with neuroblastoma. JAMA 2012;307(10):1062–1071.
72. McNicol AM. Update on tumours of the adrenal cortex, phaeochromocytoma and extra-adrenal paraganglioma. Histopathology 2011;58(2):155–168.
73. Brink I, Hoegerle S, Klisch J, Bley TA. Imaging of pheochromocytoma and paraganglioma. Fam Cancer 2005;4(1):61–68.
74. Fishbein L, Bonner L, Torigian DA, et al. External beam radiation therapy (EBRT) for patients with malignant pheochromocytoma and non-head and -neck paraganglioma: combination with 131I-MIBG. Horm Metab Res 2012;44(5):405–410.
75. Lenders JW, Duh QY, Eisenhofer G, et al. Pheochromocytoma and paraganglioma: an endocrine society clinical practice guideline. J Clin Endocrinol Metab 2014;99(6):1915–1942.
76. Mukherjee JJ, Peppercorn PD, Reznek RH, et al. Pheochromocytoma: effect of nonionic contrast medium in CT on circulating catecholamine levels. Radiology 1997;202(1):227–231.
77. Janssen I, Chen CC, Millo CM, et al. PET/CT comparing (68)Ga-DOTATATE and other radiopharmaceuticals and in comparison with CT/MRI for the localization of sporadic metastatic pheochromocytoma and paraganglioma. Eur J Nucl Med Mol Imaging 2016;43(10):1784–1791.
78. Fite JJ, Maleki Z. Paraganglioma: Cytomorphologic features, radiologic and clinical findings in 12 cases. Diagn Cytopathol 2018;46(6):473–481.

79. Barletta JA, Hornick JL. Succinate dehydrogenase-deficient tumors: diagnostic advances and clinical implications. Adv Anat Pathol 2012;19(4):193–203.
80. Allen SD, Moskovic EC, Fisher C, Thomas JM. Adult rhabdomyosarcoma: cross-sectional imaging findings including histopathologic correlation. AJR Am J Roentgenol 2007;189(2):371–377.
81. Ladra M, Marcus KJ, Yock T. Rhabdomyosarcoma. In: Terezakis SA, MacDonald SM, eds. Target Volume Delineation for Pediatric Cancers. Cham, Switzerland: Springer International, 2019; 125–144.
82. Sung CK, Kim B, Moon KC, Ku JH, Ha SB. Retroperitoneal Tumors. In: Kim SH, Cho JY, eds. Oncologic Imaging: Urology. Berlin, Germany: Springer, 2017; 227–260.
83. Feng Y. CT in Diagnosis of Retroperitoneal Tumors. In: Luo CH, ed. Retroperitoneal Tumors: Clinical Management. Dordrecht, the Netherlands: Springer Netherlands, 2018; 25–45https://doi.org/10.1007/978-94-024-1167-6_3.
84. McCarville MB. What MRI can tell us about neurogenic tumors and rhabdomyosarcoma. Pediatr Radiol 2016;46(6):881–890.
85. Kohashi K, Kinoshita I, Oda Y. Soft Tissue Special Issue: Skeletal Muscle Tumors: A Clinicopathological Review. Head Neck Pathol 2020;14(1):12–20.
86. Fletcher CD. The evolving classification of soft tissue tumours: an update based on the new WHO classification. Histopathology 2006;48(1):3–12.
87. Goldblum JR. An approach to pleomorphic sarcomas: can we subclassify, and does it matter? Mod Pathol 2014;27(Suppl 1):S39–S46.
88. Baheti AD, O'Malley RB, Kim S, et al. Soft-Tissue Sarcomas: An Update for Radiologists Based on the Revised 2013 World Health Organization Classification. AJR Am J Roentgenol 2016;206(5):924–932.
89. Lieberman PH, Brennan MF, Kimmel M, Erlandson RA, Garin-Chesa P, Flehinger BY. Alveolar soft-part sarcoma. A clinico-pathologic study of half a century. Cancer 1989;63(1):1–13.
90. Portera CA Jr, Ho V, Patel SR, et al. Alveolar soft part sarcoma: clinical course and patterns of metastasis in 70 patients treated at a single institution. Cancer 2001;91(3):585–591.
91. Folpe AL, Deyrup AT. Alveolar soft-part sarcoma: a review and update. J Clin Pathol 2006;59(11):1127–1132.
92. Itani M, Shabb NS, Haidar R, Khoury NJ. AIRP best cases in radiologic-pathologic correlation: alveolar soft-part sarcoma. RadioGraphics 2013;33(2):585–593.
93. Crombé A, Brisse HJ, Ledoux P, et al. Alveolar soft-part sarcoma: can MRI help discriminating from other soft-tissue tumors? A study of the French sarcoma group. Eur Radiol 2019;29(6):3170–3182.
94. Shah M, Freeman LM, Chitkara M, Chun KJ. Retroperitoneal hemangioma demonstrated on blood pool scan. Clin Nucl Med 2014;39(4):e265–e266.
95. Jaber OI, Kirby PA. Alveolar Soft Part Sarcoma. Arch Pathol Lab Med 2015;139(11):1459–1462.
96. Yohendran J, Dias MM, Eckstein R, Wilson T. Benign retroperitoneal cyst of Mullerian type. Asian J Surg 2004;27(4):333–335.
97. Hjermstad BM, Helwig EB. Tailgut cysts. Report of 53 cases. Am J Clin Pathol 1988;89(2):139–147.
98. Akbulut S. Unusual cause of defecation disturbance: a presacral tailgut cyst. Eur Rev Med Pharmacol Sci 2013;17(12):1688–1699.
99. Shetty AS, Loch R, Yoo N, Mellnick V, Fowler K, Narra V. Imaging of tailgut cysts. Abdom Imaging 2015;40(7):2783–2795.
100. Yang DM, Jung DH, Kim H, et al. Retroperitoneal cystic masses: CT, clinical, and pathologic findings and literature review. RadioGraphics 2004;24(5):1353–1365.
101. Francavilla ML, White CL, Oliveri B, Lee EY, Restrepo R. Intraabdominal Lymphatic Malformations: Pearls and Pitfalls of Diagnosis and Differential Diagnoses in Pediatric Patients. AJR Am J Roentgenol 2017;208(3):637–649.
102. Flors L, Leiva-Salinas C, Maged IM, et al. MR imaging of soft-tissue vascular malformations: diagnosis, classification, and therapy follow-up. RadioGraphics 2011;31(5):1321–1340; discussion 1340–1341.
103. Lal A, Gupta P, Singhal M, et al. Abdominal lymphatic malformation: Spectrum of imaging findings. Indian J Radiol Imaging 2016;26(4):423–428.
104. Ayyappan AP, Jhaveri KS, Haider MA. Radiological assessment of mesenteric and retroperitoneal cysts in adults: is there a role for chemical shift MRI? Clin Imaging 2011;35(2):127–132.
105. Kontos S, Doumanis G, Karagianni M, et al. Burned-out testicular tumor with retroperitoneal lymph node metastasis: a case report. J Med Case Reports 2009;3(1):8705.